The viscous Cahn-Hilliard equation. I. Computations

1995 Nonlinearity 8 131

Nonlinearity 8 (1995) 131–160. Printed in the UK

The viscous Cahn–Hilliard equation. Part I: computations

F Bai†‖ ¶ +, C M Elliott‡+, A Gardiner‡+, A Spence†+ and A M Stuart§*

† School of Mathematical Sciences, University of Bath, Bath, BA2 7AY, UK

‡ Center for Mathematical Analysis and Its Applications, University of Sussex, Brighton BN1 9QH, UK

§ Division of Applied Mechanics,Durand 252, Stanford University, Stanford CA 94305-4040, USA

Received 16 November 1993, in final form 27 September 1994
Recommended by J D Gibbon

Abstract. The viscous Cahn–Hilliard equation arises as a singular limit of the phase-field model of phase transitions. It contains both the Cahn–Hilliard and Allen–Cahn equations as particular limits. The equation is in gradient form and possesses a compact global attractor $\mathcal{A}$, comprising heteroclinic orbits between equilibria.

Two classes of computation are described. First heteroclinic orbits on the global attractor are computed; by using the viscous Cahn–Hilliard equation to perform a homotopy, these results show that the orbits, and hence the geometry of the attractors, are remarkably insensitive to whether the Allen–Cahn or Cahn–Hilliard equation is studied. Second, initial-value computations are described; these computations emphasize three differing mechanisms by which interfaces in the equation propagate for the case of very small penalization of interfacial energy. Furthermore, convergence to an appropriate free boundary problem is demonstrated numerically.

AMS classification scheme numbers: 35K35, 65N25, 65N35, 65M99.

1. Introduction

In this paper we study the viscous Cahn–Hilliard equation [27] written in the form

$$u_t = \Delta w \qquad x \in \Omega \qquad t > 0, \tag{1.1}$$

$$\alpha u_t = \gamma \Delta u + f(u) + \beta w \qquad x \in \Omega \qquad t > 0 \tag{1.2}$$

with initial condition

$$u(x, 0) = u_0(x) \qquad x \in \Omega. \tag{1.3}$$

We consider either the case of Dirichlet boundary conditions so that

$$u = w = 0 \qquad x \in \partial\Omega \qquad t > 0 \tag{1.4}$$

‖ Also at: Program in Scientific Computing and Computational Mathematics, Stanford University, CA 94305, USA

¶ On leave from: Applied Mathematics Department, Tsinghua University, Beijing 100084, People's Republic of China

+ Work supported by UK Science Engineering Research Council grants.

* Work supported by the Office of Naval Research and the National Science Foundation under contracts N00014-92-J-1876 and DMS-9201727 respectively.

0951-7715/95/020131+30$19.50

or Neumann boundary conditions so that

$$\frac{\partial u}{\partial n} = \frac{\partial w}{\partial n} = 0 \qquad x \in \partial\Omega \qquad t > 0 \tag{1.5}$$

where n denotes the unit outward normal on Ω. In the latter case we also impose mass conservation

$$\int_\Omega u(x,t)\mathrm{d}x = \int_\Omega u(x,0)\mathrm{d}x \qquad \forall t > 0 \tag{1.6}$$

so that (1.1) is uniquely solvable for w in terms of u_t. Throughout, Ω is a bounded domain in $\mathbb{R}^d$ $(d = 1, 2, 3)$, $\gamma \in (0, \infty)$, $\alpha \geqslant 0, \beta \geqslant 0$ and

$$f(s) = \sum_{j=1}^{2p-1} b_j s^j \qquad b_{2p-1} < 0. \tag{1.7}$$

In the context of this paper, the importance of the parameters α, β is to distinguish three cases: (i) $\alpha = 0, \beta \neq 0$, (ii) $\alpha \neq 0, \beta = 0$ and (iii) α and β both $\neq 0$. In the case (*i*) equations (1.1), (1.2) reduce to the Cahn–Hilliard model for spinodal decomposition—a description of the process by which phase separation occurs in a binary alloy after the temperature is reduced beneath its critical value, [10]. In case (ii) we obtain the Allen–Cahn model for grain-boundary migration, the process by which the interface between two differently aligned crystal lattices in a solid evolve with time, [2]. The viscous Cahn–Hilliard equation, obtained in case (iii), is derived in [27] to include certain viscous effects neglected in [10]. It is our purpose to study the similarities and differences between the two cases (i) and (ii) by use of case (iii) to interpolate between them.

In section 2 we describe how the viscous Cahn–Hilliard equation can be derived from the phase-field equations. The phase-field equations can themselves be derived in a thermodynamically consistent manner [30] so that this gives the physical motivation for our investigation of equations (1.1)–(1.3). In sections 3,4 and 5 we find it convenient to set $\beta = 1 - \alpha$ and consider $\alpha \in [0, 1]$. It is then clear that α acts as a 'continuation' parameter taking the Cahn–Hilliard equation ($\alpha = 0$) to the Allen–Cahn equation ($\alpha = 1$) and we interpret the viscous Cahn–Hilliard equation as interpolating between these equations for $\alpha \in (0, 1)$. The particular choice of parameters $\beta = 1 - \alpha$ appears somewhat special but enables us to consider a one parameter homotopy between the two models which encapsulates cases (i), (ii) and (iii). In section 3 we study the properties of equilibria of (1.1)–(1.3) under Dirichlet boundary conditions; note that the equilibria themselves are independent of α and our study thus concentrates on stability questions. Section 4 is concerned with the properties of equations (1.1)–(1.3) on the global attractor $\mathcal{A}$, also for Dirichlet boundary conditions. By virtue of the gradient structure inherent in (1.1)–(1.3) this reduces to the study of the properties of heteroclinic orbits: these are solutions of (1.1)–(1.3) which are asymptotic to equilibrium solutions as $t \to \pm\infty$. Our computations demonstrate that these orbits are remarkably insensitive to changes in $\alpha \in [0, 1]$, thus showing a strong connection between the attractors of the Cahn–Hilliard and Allen–Cahn models. In section 5 the observations of section 4 are extended to the case of Neumann boundary conditions.

Whilst sections 3–5 are concerned with highlighting the remarkable similarities between the Cahn–Hilliard and Allen–Cahn models, by setting $\beta = 1 - \alpha$ in (1.1) and using α as a homotopy parameter, section 6 shows that important differences remain. By scaling α, β and γ with respect to a small parameter ε it is possible to recover a variety of physically meaningful free boundary problems in the limit $\varepsilon \to 0$ and the differences between the cases (i), (ii) and (iii) are highlighted. Specifically this section is concerned with initial value computations designed to show the three very different mechanisms by which interfaces

propagate, depending upon values of α and β. Both Dirichlet and Neumann boundary conditions are considered.

2. Relationship to phase-field models

The phase-field equations are

$$c\theta_t + \frac{l}{2}u_t = k\Delta\theta \qquad x \in \Omega \qquad t > 0 \tag{2.1}$$

$$\alpha u_t = \gamma\Delta u + f(u) + \delta\theta \qquad x \in \Omega \qquad t > 0. \tag{2.2}$$

We consider these equations subject to either the Dirichlet boundary conditions

$$u = \theta = 0 \qquad x \in \partial\Omega \qquad t > 0 \tag{2.3}$$

or Neumann boundary conditions so that

$$\frac{\partial u}{\partial n} = \frac{\partial\theta}{\partial n} = 0 \qquad x \in \partial\Omega \qquad t > 0 \tag{2.4}$$

where n denotes the unit outward normal on Ω. These equations arise in the modelling of solidification of supercooled liquids—see Caginalp [6], Penrose and Fife [30] and Caginalp and Fife [7]. Here θ and u are the temperature and phase variables. The positive constants c, l and k denote, respectively, the specific heat, latent heat and thermal conductivity. The positive constants α, γ and δ may be chosen to scale with a small parameter ε to yield physically meaningful free boundary limits as $\varepsilon \to 0$; see section 6 and Caginalp and Fife [7]. Here $f(u)$ is chosen so that $F(\cdot)$ given by $F'(u) = -f(u)$ is an equal double well potential which has two global minima at ± 1. The simplest example is $f(u) = u - u^3$. By a suitable choice of parameters one may recover from (2.1), (2.2) a variety of parabolic systems arising in the modelling of diffusive phase transformations in alloys.

By setting $c = 0$ and defining

$$\beta = \frac{\delta l}{2k} \qquad \text{and} \qquad \theta = \frac{l}{2k}w \tag{2.5}$$

we recover the viscous Cahn-Hilliard equation (1.1), (1.2) from the phase-field equations.

By setting $c = \alpha = 0$ in (2.1), (2.2) and eliminating θ we obtain the Cahn–Hilliard equation, (see [9, 10, 15])

$$\frac{\delta l}{2k}u_t = -\gamma\Delta^2 u - \Delta f(u). \tag{2.6}$$

This equation is usually solved subject to the boundary conditions

$$u = \Delta u = 0 \qquad x \in \partial\Omega \qquad t > 0 \tag{2.7}$$

(which follow from (2.3) for the phase-field equations) or the homogeneous Neumann boundary conditions

$$\frac{\partial u}{\partial n} = \frac{\partial}{\partial n}(\Delta u) = 0 \tag{2.8}$$

(which follows from (2.4) for the phase-field equations).

If we set $c = l = 0$ in (2.1), (2.2) and impose the boundary conditions (2.3) we obtain (using uniqueness of solutions to the homogeneous Laplacian problem) the Allen–Cahn equation (see [2]),

$$\begin{aligned} &\alpha u_t = \gamma\Delta u + f(u) \qquad x \in \Omega \qquad t > 0 \\ &u = 0 \qquad x \in \partial\Omega \qquad t > 0. \end{aligned} \tag{2.9}$$

Equation (2.9) is also known as the Chafee–Infante equation, (see [11, 23]) when it is usually studied in the form obtained by dividing through by γ $(= \lambda^{-1})$ and rescaling time.

If, instead of (2.3), we employ homogeneous Neumann conditions (2.4), impose mass conservation and set $c = l = 0$ then (2.1), (2.2) becomes the non-local Allen–Cahn equation, (Rubenstein and Sternberg [31])

$$\begin{aligned} &\alpha u_t = \gamma \Delta u + f(u) - \frac{1}{|\Omega|}\int_\Omega f(u(x))dx \qquad x \in \Omega \qquad t > 0 \\ &\frac{\partial u}{\partial n} = 0 \qquad x \in \partial\Omega \qquad t > 0. \end{aligned} \tag{2.10}$$

Since the viscous Cahn–Hilliard equation arises from the phase-field model by setting $c = 0$ it may be viewed as a singular limit. Another way to see this is to derive from (2.1), (2.2) a damped wave equation and show how the viscous Cahn–Hilliard equation arises from it. Applying $-\Delta$ to both sides of (2.2), we obtain

$$-\alpha \Delta u_t = -\gamma \Delta^2 u - \Delta f(u) - \delta \Delta \theta$$

and eliminating $\Delta\theta$ by using (2.1) yields

$$-\alpha \Delta u_t + \frac{\delta}{k} c\theta_t + \frac{\delta}{k}\frac{l}{2} u_t = -\gamma \Delta^2 u - \Delta f(u). \tag{2.11}$$

Differentiating (2.2) with respect to t and substituting into (2.11) yields a single damped wave equation for u, that is

$$c\alpha u_{tt} - (k\alpha + c\gamma)\Delta u_t + \left(\frac{l\delta}{2} - cf'(u)\right) u_t = -k\gamma \Delta^2 u - k\Delta f(u). \tag{2.12}$$

Setting $c = 0$ and using (2.5) to define β we obtain

$$\beta u_t - \alpha \Delta u_t = -\gamma \Delta^2 u - \Delta f(u) \qquad x \in \Omega \qquad t > 0 \tag{2.13}$$

for the phase variable $u(x, t)$. This is the form of the viscous Cahn–Hilliard equation originally derived in [27] and can be derived from (1.1), (1.2) by eliminating w.

Thus the phase-field equations (2.1), (2.2) contain a variety of interesting equations in particular parameter limits. Related observations are made in [14].

3. Analysis of the steady state

Here we consider the existence and stability of equilibria for equations (1.1)–(1.4) in the case $\beta = 1 - \alpha$ and $\alpha \in [0, 1]$. In the following we use $|\bullet|$ to denote the standard $L^2(\Omega)$ norm and $\|\bullet\|$ the standard $H^1(\Omega)$ norm. The usual theory for the solution of second-order boundary value problems of the form

$$\begin{aligned} &-\gamma \Delta u - qu = f \qquad x \in \Omega \\ &u = 0 \qquad x \in \partial\Omega \end{aligned} \tag{3.1}$$

with $q \in C(\bar{\Omega})$ involves the introduction of a solution operator $\mathcal{G}$, such that $u = \mathcal{G}f$, with the property that $\mathcal{G} : L^2(\Omega) \to H^2(\Omega) \cap H_0^1(\Omega)$. Hence $\mathcal{G}$ is compact on both $L^2(\Omega)$ and $H^1(\Omega)$. Also $\mathcal{G}$ is self-adjoint on both spaces.

In the case $\gamma = 1, q(x) \equiv 0$ in (3.1) we denote the solution operator by $\mathcal{G}_0$. Hence (1.1) and (1.4) yields

$$w = -\mathcal{G}_0 u_t. \tag{3.2}$$

Now let $\beta = (1 - \alpha)$. After introducing B_α, a bounded, self-adjoint, positive operator on $H^1(\Omega)$ given by

$$B_\alpha := \alpha I + (1 - \alpha)\mathcal{G}_0, \tag{3.3}$$

(1.2) becomes

$$B_\alpha u_t = \gamma \Delta u + f(u) \qquad x \in \Omega \qquad t > 0 \tag{3.4}$$

with boundary condition

$$u = 0 \qquad x \in \partial\Omega \qquad t > 0 \tag{3.5}$$

and initial condition

$$u(x, 0) = u_0(x) \qquad x \in \Omega. \tag{3.6}$$

For $\alpha = 0$ or 1 the existence theory for (3.4)–(3.6) is well known, [11, 23, 19, 33]. For $\alpha \in (0, 1)$, it is developed in [18] and [27]. In summary these references show that, for all $\alpha \in [0, 1]$, (3.4)–(3.6) generates a semigroup $S^\alpha(u, t) \in C^1(H_0^1(\Omega) \times \mathbb{R}^+, H_0^1(\Omega))$ so that $u(t) = S^\alpha(u_0, t)$.

Note that (1.7) implies the existence of a constant C_f and a non-negative function $F(\cdot)$ such that

$$f'(s) \leqslant C_f \qquad f(s) = -F'(s) \qquad \forall s \in \mathbb{R}. \tag{3.7}$$

Given this function F observe that solutions of (3.4)–(3.6) are in gradient form: defining

$$\mathcal{V}(\phi) = \int_\Omega \{\frac{\gamma}{2}|\nabla\phi|^2 + F(\phi)\}dx \tag{3.8}$$

we have

$$\frac{d}{dt}\{\mathcal{V}(u(t))\} = - \mid u_t(t) \mid_B^2 .$$

Here $|\bullet|_B$ is the norm induced by B_α, namely

$$|v|_B^2 = \langle v, v\rangle_B, \langle u, v\rangle_B := \langle u, B_\alpha v\rangle.$$

Note that $|\bullet|_B$ is equivalent to the norm on $L^2(\Omega)$ for $\alpha \in (0, 1]$ and to the $H^{-1}(\Omega)$ norm for $\alpha = 0$.

Using the gradient structure of the equations, it is shown in [18] that, provided all equilibria are hyperbolic, the equations (3.4) and (3.5) have a global attractor $\mathcal{A}$ which is formed as the union of heteroclinic orbits between equilibria. Heteroclinic orbits are solutions of (3.4) and (3.5) which satisfy boundary conditions in time of the form

$$u(t) \to u_\pm \quad \text{as} \quad t \to \pm\infty \tag{3.9}$$

where $u_\pm \in \mathcal{E}$, the set of equilibria of (3.4)–(3.6). Thus heteroclinic orbits are solutions of (3.4) and (3.5) on the infinite cylinder $(x, t) \in \Omega \times \mathbb{R}$. The equilibrium solution u_-, observed as $t \to -\infty$, is known as an alpha-limit set. Likewise, u_+ is known as an omega-limit set. (The use of alpha in this context should not be confused with the parameter α appearing in the model (1.1)– (1.3).) Thus to study the attractor it is sufficient to compute heteroclinic orbits of (3.4) and (3.5).

In order to implement the numerical method described in section 4 for the computation of heteroclinic orbits satisfying (3.4), (3.5) and (3.9) it is necessary to compute the equilibria of (3.4), (3.5) and also to determine the linearized stable and unstable manifolds of the equilibria. The remainder of this section is devoted to a study of the equilibria of (3.4), (3.5) and their stability properties.

From (3.4), (3.5) it is clear that equilibria $\bar{u}$ of the viscous Cahn–Hilliard equation satisfy the semilinear elliptic equation

$$\begin{aligned} &\gamma\Delta\bar{u} + f(\bar{u}) = 0 \qquad x \in \Omega \\ &\bar{u} = 0 \qquad x \in \partial\Omega \end{aligned} \tag{3.10}$$

and hence are independent of α. It is our purpose in this section to prove that the qualitative stability properties of the equilibria $\bar{u}$ are also independent of $\alpha \in [0, 1]$. Specifically we show that the dimension of the unstable manifold of $\bar{u}$ is independent of $\alpha \in [0, 1]$ (theorem 3.1) and that the linearized unstable manifold is a smooth function of α (theorem 3.2). From the formulation of (3.4), (3.5) using the theory of analytic semigroups (see Elliott and Stuart [18]) it follows that the principle of linearized stability [23] holds for the equations. Thus stability of $\bar{u}$ is governed by the eigenvalues ρ and eigenfunctions ϕ of the problem

$$\rho\phi = B_\alpha^{-1}[\gamma\Delta\phi + f'(\bar{u})\phi] \qquad x \in \Omega \tag{3.11}$$

$$\phi = 0 \qquad x \in \partial\Omega. \tag{3.12}$$

Let $q(x) := f'(\bar{u}(x))$ in (3.11) and let $\mathcal{G}_1$ denote the corresponding solution operator for the problem (3.1). From now on we assume that the equilibria $\bar{u}$ are hyperbolic so that the operator $-\gamma\Delta - qI$ is invertible on $L^2(\Omega)$. Hence we are looking at the case where (3.11) and (3.12) has no zero eigenvalues for all $\alpha \in [0, 1]$. We see that weak solutions of (3.11) and (3.12) satisfy

$$\rho\mathcal{G}_1 B_\alpha\phi + \phi = 0 \qquad \phi \in H^1(\Omega). \tag{3.13}$$

Note that for $\alpha = 1$ there are a finite number of positive eigenvalues of (3.13).

Now since $\mathcal{G}_1$ is compact on $H^1(\Omega)$ and B_α is bounded on $H^1(\Omega)$ we deduce that $\mathcal{G}_1 B_\alpha$ is a family of compact operators on $H^1(\Omega)$, and moreover for all $\alpha, \alpha+\varepsilon \in [0, 1]$ we have from (3.3) that

$$\mathcal{G}_1 B_{\alpha+\varepsilon} - \mathcal{G}_1 B_\alpha = \varepsilon\mathcal{G}_1(I - \mathcal{G}_0). \tag{3.14}$$

Using (3.13), (3.14) we develop a theory of the invariance of the number of positive eigenvalues of (3.13) as a function of α. For any fixed $\alpha \in [0, 1]$, $\mathcal{G}_1$ and B_α satisfy the conditions on L and M (respectively) in theorem A of the appendix. Using this theorem we obtain:

Theorem 3.1. *Assume that for $\alpha = 1$ the eigenvalue problem (3.13) has exactly m positive eigenvalues. Then for each $\alpha \in [0, 1]$, the eigenvalue problem (3.13) has exactly m positive semisimple eigenvalues (counting using multiplicities).*

For each $\alpha \in [0, 1]$, let $\mathcal{P}_+^\alpha$ denote the spectral projection in $H^1(\Omega)$ of the eigenspace corresponding to the positive eigenvalues of (3.13). Then theorem 3.1 implies

$$\dim(\mathcal{P}_+^\alpha H^1(\Omega)) = m \qquad \forall\alpha \in [0, 1].$$

Now the perturbation theory results given by theorems 5 and 6 (with ascent=1) in [28] applied to $\mathcal{G}_1 B_{\alpha+\varepsilon}$ show the smoothness with respect to α of the eigenspace corresponding to the m positive eigenvalues:

Theorem 3.2. *There exists $C > 0$ such that, for all α, ε: $\alpha, \alpha + \varepsilon \in [0, 1]$,*

$$\|\mathcal{P}_+^{\alpha+\varepsilon} - \mathcal{P}_+^\alpha\| \leqslant C\varepsilon.$$

Furthermore, if the eigenvalues ρ^α of (3.13) are simple then

$$|\rho^{\alpha+\varepsilon} - \rho^\alpha| \leqslant C\varepsilon.$$

Theorem 3.1 shows that the dimension of the unstable manifold of an equilibrium solution $\bar{u}$ of (3.4), (3.5) is independent of α. Furthermore, theorem 3.2 establishes the continuity of the linearized unstable manifold with respect to α. With this knowledge, we now proceed to compute heteroclinic connections between equilibria and in particular, study how they vary with α. (Before doing this it is worth remarking that the above theory does not rely on the relation $\beta = (1-\alpha)$. We could define an operator $B_{\alpha,\beta}$ by $B_{\alpha,\beta} = \alpha I + \beta \mathcal{G}_0$ and develop a theory of equilibria of (1.1)–(1.3) accordingly. Invariance and continuity theorems, with respect to α and β, similar to those stated here for the case $\beta = 1-\alpha$, may be obtained.)

For computational purposes we shall study (3.4), (3.5) with

$$f(u) = u - u^3 \tag{3.15}$$

in the remainder of this paper. Furthermore, in sections 3,4 and 5 we will consider $\Omega = (0, 1) \subset \mathbb{R}$. In section 6 we will consider both one- and two-dimensional computations.

If $\Omega = (0, 1)$ and (3.15) holds then the steady-state bifurcation diagram is well-known [11] —see Figure 3.1.

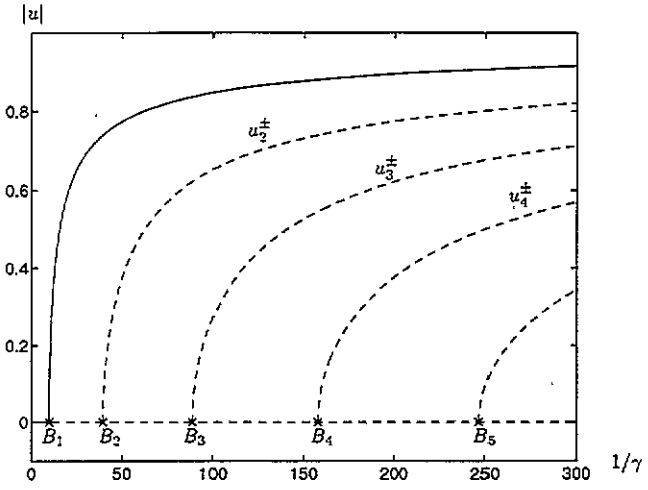

Figure 3.1. The steady state solutions for viscous Cahn–Hilliard equation (3.4), (3.5); — denotes stable branches, and ----- denotes unstable branches.

Furthermore, for $\alpha = 1$ in (3.4), (3.5) the stability properties of all the steady state solutions have been determined in [11, 23, 24]. Using theorem 3.1, these can be extended to all $\alpha \in [0, 1]$. Thus we obtain:

Theorem 3.3. *Assume that $f(u) = u - u^3$, $\Omega = (0, 1) \subset \mathbb{R}$. For each integer $k \geqslant 1$ and $\gamma^{-1} \in (k^2\pi^2, +\infty)$, equations (3.4), (3.5) have two nonzero equilibrium points with $k-1$ interior zeros, denoted $u_k^{\pm}(\gamma)$. These are the only equilibria with $k-1$ interior zeros. Here $u_k^+(\gamma) = -u_k^-(\gamma)$ and the argument γ denotes the dependence of the equilibria on γ. The following properties hold for these equilibria:*

(a) For $\gamma^{-1} \in (0, k^2\pi^2)$ equations (1.1)—(1.2) have no equilibrium points other than $u \equiv 0$ and $u_j^{\pm}(\gamma)$, $j < k$.

(b) Let $\alpha \in [0, 1]$. Then, for each $\gamma^{-1} \in (0, \pi^2)$, the solution $u \equiv 0$ is asymptotically stable and for each $\gamma^{-1} \in (\pi^2, +\infty)$ $u \equiv 0$ is unstable. Furthermore, for any $\alpha \in [0, 1]$, the dimension of the unstable manifold equals k for $\gamma^{-1} \in (k^2\pi^2, (k+1)^2\pi^2)$.

(c) Let $\alpha \in [0, 1]$. Then, for each $k \geqslant 1$ and any $\gamma^{-1} \in (\pi^2, +\infty)$ the equilibrium point $u_1^{\pm}(\gamma)$ is asymptotically stable. For any $\gamma^{-1} \in (k^2\pi^2, +\infty)$, $k > 1$, the equilibrium point $u_k^{\pm}(\gamma)$ is unstable and the dimension of the unstable manifold is $k - 1$.

4. Numerical method and results

In this section we present numerical computations which indicate that the global attractor for the viscous Cahn–Hilliard equation is qualitatively insensitive to changes in the parameter α. Since the equation is in gradient form (see section 3), to study the attractor it is sufficient to study the behaviour of heteroclinic orbits satisfying (3.4), (3.5) and (3.9)—see [22] and [33]; the work of [33] (and the references therein) in particular contains discussion of various properties of the attractor for the case $\alpha = 0$ and Neumann boundary conditions. The structure of the attractor is completely understood for $\alpha = 1$ and Dirichlet boundary conditions as a consequence of the work of [23, 24]—that is, the question of whether there exists a heteroclinic orbit connecting any given pair of equilibria is answered, and the number of parameters required to describe each such connection is known.

A numerical method appropriate for the calculation of heteroclinic orbits in partial differential equations in gradient form was developed in [3]; the numerical method we use here is based on [3] and we only briefly describe the computational technique. Other computations for connecting orbits are described, for example, in [21]. The infinite cylinder is replaced by the truncated domain $(x, t) \in \Omega \times (-T, T)$, for some large $T \gg 1$ and (3.9) is replaced by boundary conditions

$$\mathcal{P}_+[u(T) - u_+] = 0 \qquad \mathcal{P}_-[u(-T) - u_-] = 0. \tag{4.1}$$

Here $\mathcal{P}_+$ (respectively $\mathcal{P}_-$) is a projection onto the unstable (stable) manifold of u_+ (u_-). This approach is used in Beyn [5]. To eliminate translation invariance it is also necessary to impose a phase condition and it may be necessary to supplement (4.1) with further conditions to yield a well-posed boundary value problem in time with the correct number of boundary conditions; see [3] to see how this may be done.

We approximate (3.4), (3.5) by a Galerkin spectral method, setting

$$u_N(x, t) = \sum_{j=1}^{N} a_j(t) \sin(j\pi x). \tag{4.2}$$

Thus

$$\mathcal{G}_0 u_N(x, t) = \sum_{j=1}^{N} \frac{a_j(t)}{j^2\pi^2} \sin(j\pi x).$$

Substituting into (3.4) and applying Galerkin projection, gives

$$\left\{\alpha + \frac{1-\alpha}{k^2\pi^2}\right\} \frac{da_k(t)}{dt} = -\gamma a_k(t)\pi^2 k^2 + g_k(A) \tag{4.3}$$

where $A = (a_1, a_2, \cdots, a_N)$ and

$$g_k(A) = 2\int_0^1 f(u_N(x, t)) \sin(k\pi x) dx.$$

Thus we obtain a system of ordinary differential equations for A. This system is parametrized by α and is also in gradient form. All computations are performed with values of N between 20 and 50 and have been checked for consistency by employing a variety of different choices of N.

The steady state of the semidiscrete problem (4.3) is independent of α, as for the equations (3.4), (3.5). Furthermore, in the finite dimensional setting, theorems 3.1 and 3.2 may be modified to cover both positive and negative eigenvalues for the semidiscrete problem, and hence we know that the dimension of the stable and unstable manifolds of (4.3) are independent of α. Thus provided that N is sufficiently large so that the eigenspaces of (3.4), (3.5) are well-approximated, the existence and stability properties of steady states implied by theorem 3.3 will be inherited by a semidiscrete approximation provided attention is restricted to a compact interval of positive γ^{-1} and a compact region of phase space. This is confirmed by numerical results.

We now proceed to compute heteroclinic connections. We show that, in terms of the geometry of the connections, the computations show a remarkable insensitivity to the parameter α, though the time scales (which are partially governed by the eigenvalues of the linearizations) are very different. Figure 4.1(i), (a) shows how the first eigenvalue, ρ_1^α on u_2^+ at $\gamma^{-1} = 130$, changes as α varies from 0 to 1; (b) shows the same for ρ_2^α. This verifies theorem 3.2 which shows that the eigenvalues change smoothly with respect to α. The same is true for the eigenfunctions, although we only give results for the two values $\alpha = 0, 1$. In figure 4.1(ii) we consider the eigenfunctions arising from linearization of u_2^+. figure 4.1(ii) (a) shows the eigenfunction, ϕ_1^α, of the Allen–Cahn problem corresponding to ρ_1^α with $\alpha = 1$; (b) is that of the Cahn–Hilliard equation corresponding to ρ_1^α with $\alpha = 0$. Note that for this value of γ these eigenfunctions determine the one-dimensional linearized unstable manifold of u_2^+. Figures (c) and (d), (e) and (f), and (g) and (h) are similar plots for the eigenfunctions ϕ_2^α, ϕ_3^α and ϕ_4^α, corresponding to ρ_2^α, ρ_3^α and ρ_4^α respectively, again alternating the Allen–Cahn and Cahn–Hilliard cases. Comparison shows that not only are the dominant eigenfunctions smooth functions of α but also that they are remarkably insensitive to $\alpha \in [0, 1]$. Since the heteroclinic orbits are formed as intersections of unstable manifolds it perhaps not surprising that they too are insensitive to α. We now show this numerically.

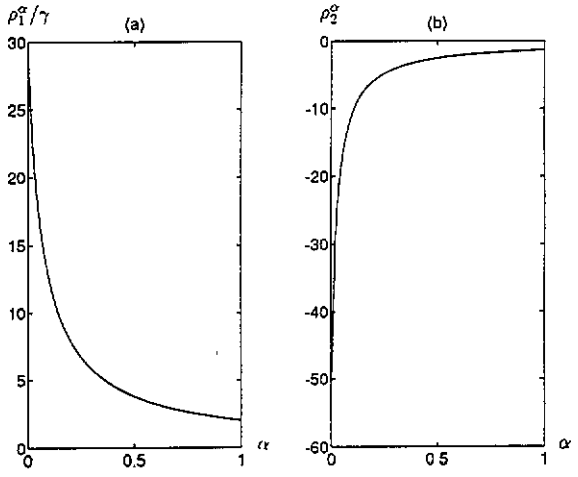

Figure 4.1.(i). eigenvalues changing with α at $\gamma^{-1} = 130$ for u_2^+. $\alpha = 0$ is Cahn–Hilliard;$\alpha = 1$ is Allen–Cahn.

Throughout the following we use the notation $u_k^\pm(\gamma)$ as detailed in theorem 3.3 for steady solutions of the problem. In the heading of the subsections, *alpha*(•) and *omega*(•) denote the alpha and omega limit sets of the computed heteroclinic orbit respectively. (See

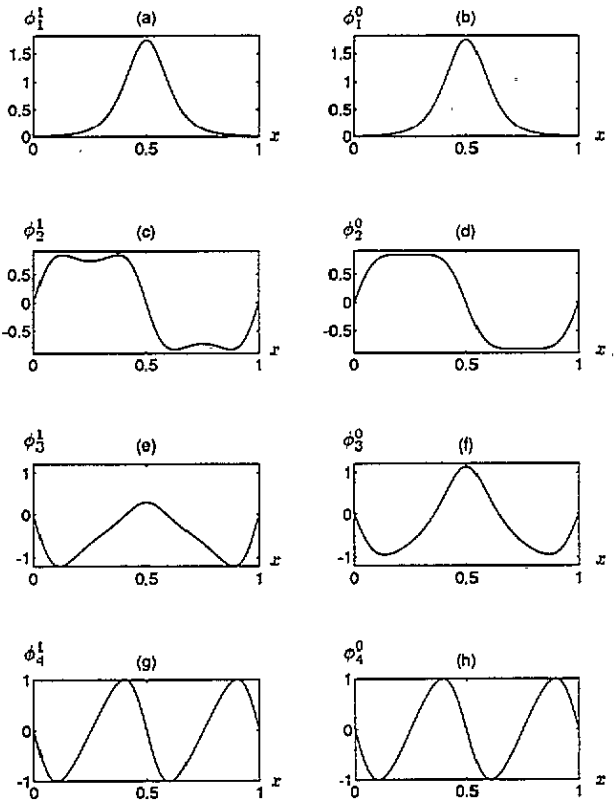

Figure 4.1.(ii). eigenfunctions for $\alpha = 0$ and 1 at $\gamma^{-1} = 130$ for $u_2^{\pm}$. (a), (c), (e), (g) Allen–Cahn, $\alpha = 1$; (b), (d), (f), (h) Cahn–Hilliard, $\alpha = 0$.

section 3 for a definition of these objects and recall that alpha in this context should not be confused with the parameter α appearing in the equations.)

4.1. alpha $(u(0)) = 0$, *omega*$(u(0)) = u_2^{\pm}(\gamma), \gamma^{-1} = 130$

For $\gamma^{-1} = 130$, we have $9\pi^2 < \gamma^{-1} < 16\pi^2$. In the case $\alpha = 1$, (the Allen–Cahn equation), the connections between u_0 and $u_2^{\pm}(\gamma)$ form a manifold of dimension 2 [23, 24]. One of these parameters is simply time; as the second we take

$$\mu := \int_0^1 [a_3(\tau)]^2 \mathrm{d}\tau \tag{4.4}$$

as in [3], to parametrize the manifold. Here τ is a linear re-scaling of time employed so that all computations of heteroclinic orbits performed on $t \in [-T, T]$ by virtue of (4.1), are rescaled to the unit interval $\tau \in [0, 1]$. Using the techniques described in [3] we may find a heteroclinic connection between $u \equiv 0$ and $u_2^{\pm}(\gamma)$ for any value of μ. Note that, since $u_2^{\pm}$ is unstable, such a connection is unstable as a solution of the initial-value problem so that it cannot be computed by standard forward integration in time of the initial-value problem. This is why a technique based on solving a boundary-value problem in space and time is used.

For any fixed μ, we can compute connecting orbits for the viscous Cahn–Hilliard equation, using α as the continuation parameter. The package AUTO [12] is used to

perform the continuation.

Figures 4.2(i) and (ii) show (time rescaled) plots of the heteroclinic orbits for Allen–Cahn and Cahn–Hilliard equations respectively. The plot corresponds to an order-preserving time reparametrization induced by the choice of collocation points in AUTO [12]. Equal spacing in $s \in [0, 1]$ is equivalent to a variable mesh in $\tau \in [0, 1]$ chosen by AUTO. Thus, since τ is a linear re-scaling of t we deduce that $s = \chi(t)$, for some monotonic increasing $\chi(\cdot)$. The true time scale can be recovered from figures 4.3(i) and (ii), where the 'o's demark intervals in time equidistributed in figures 4.2(i) and (ii). Comparison of figures 4.2(i) and 4.2(ii) and 4.3(i) and (ii) shows the insensitivity of the heteroclinic orbits (and hence the attractor) for the viscous Cahn–Hilliard equation to the parameter α. Qualitatively the heteroclinic orbits are independent of α. In fact after rescaling time the orbits are almost indistinguishable. Figure 4.4 plots the difference, denoted e, between two heteroclinic connections for two nearby parameters $\alpha_1 = 0$ (Cahn–Hilliard equation) and $\alpha_2 = 3.13 \times 10^{-4}$; this figure shows the continuity of the heteroclinic connection with respect to α.

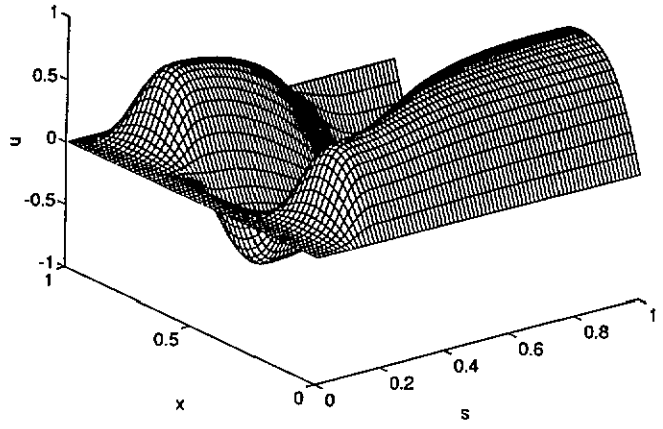

Figure 4.2.(i). $1/\gamma = 130, \mu = 0.5000, \alpha = 1$, the Allen–Cahn equation. $s = \chi(t)$.

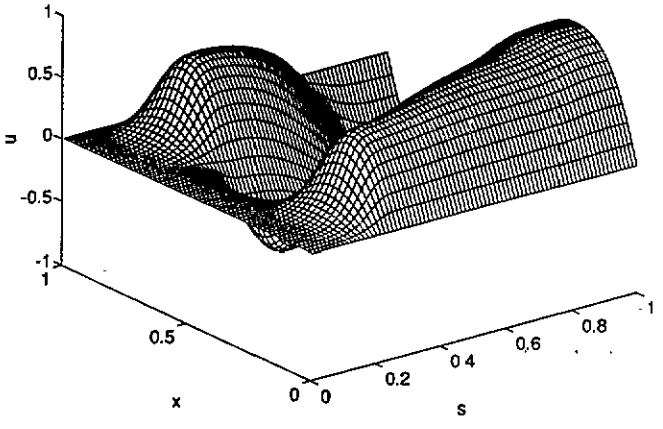

Figure 4.2.(ii). $1/\gamma = 130, \mu = 0.5000, \alpha = 0$, the Cahn–Hilliard equation. $s = \chi(t)$.

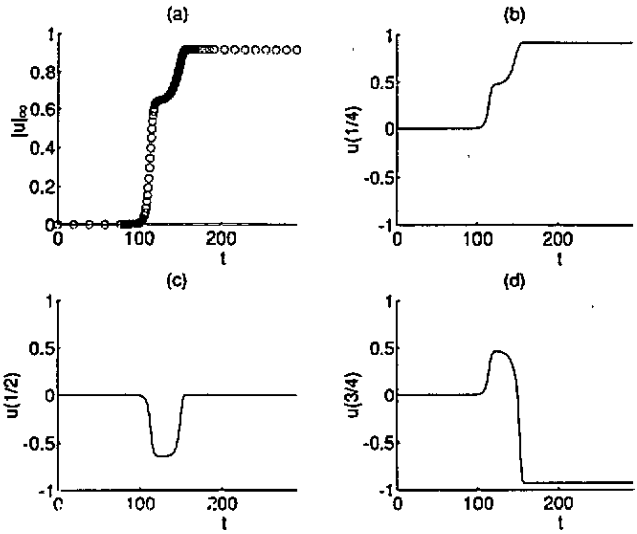

Figure 4.3.(i). The Allen–Cahn equation, $\alpha = 1$. $1/\gamma = 130$, $\mu = 0.5000$. The argument of u denotes the x variable.

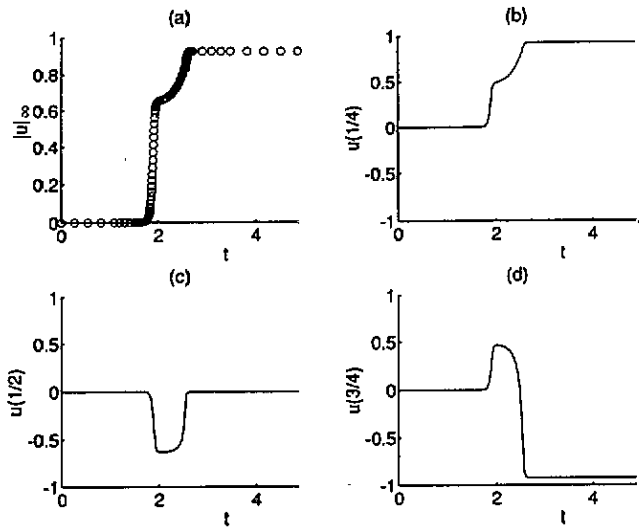

Figure 4.3.(ii). The Cahn–Hilliard equation, $\alpha = 0$. $1/\gamma = 130$, $\mu = 0.5000$. The argument of u denotes the x variable.

4.2. alpha$(u(0)) = 0$, *omega*$(u(0)) = u_2^{\pm}(\gamma)$, $\gamma^{-1} = 190$

For $\gamma^{-1} = 190$, we have $16\pi^2 < \gamma^{-1} < 25\pi^2$. The connections between u_0 and $u_2^{\pm}(\gamma)$ form a manifold of dimension 3. We take the parameters

$$\mu_1 = \int_0^1 [a_3(s)]^2 ds \tag{4.5}$$

$$\mu_2 = \int_0^1 [a_4(s)]^2 ds \tag{4.6}$$

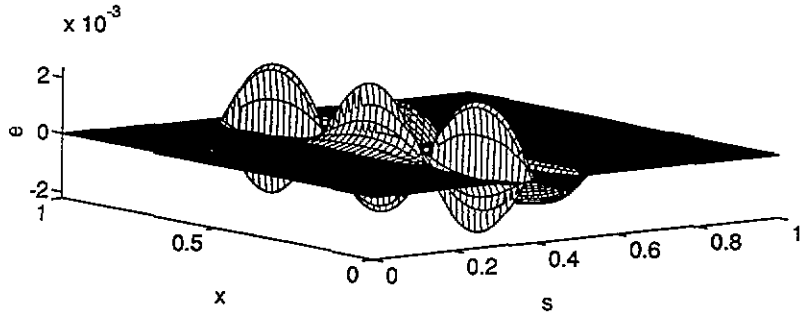

Figure 4.4. $1/\gamma = 130, \mu = 0.5000, \alpha_1 = 0.0000, \alpha_2 = 3.13 \times 10^{-4}$. $e = u(x, s; \alpha_1) - u(x, s; \alpha_2), s = \chi(t)$.

together with time t, to parametrize this manifold. As before we can compute a heteroclinic orbit for any given value of μ_1 and μ_2 by using the techniques of [3]. After computing a given connecting orbit for the Allen–Cahn problem for a particular μ_1 and μ_2, we compute connecting orbits for the viscous Cahn–Hilliard equation using α as a continuation parameter. Such results are shown in figures 4.5. Further quantitative agreement maybe be observed by more detailed comparison of the connecting orbits.

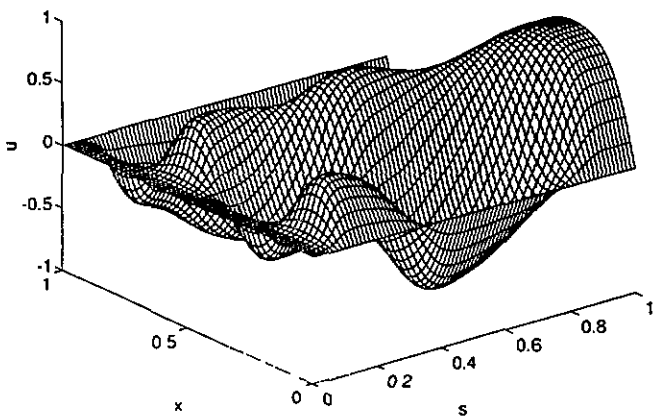

Figure 4.5.(i). $1/\gamma = 190, \mu_1 = 0.3688, \mu_2 = 0.1850, \alpha = 1$, the Allen–Cahn problem. $s = \chi(t)$.

In summary we have shown that the global attractor for (3.4), (3.5), (3.6) is insensitive to α. Since the physically interesting behaviour of the equation is confined to the attractor, this observation implies that, at a qualitative level, the value $\alpha \in [0, 1]$ plays no role.

5. Neumann boundary conditions

Here we study the viscous Cahn–Hilliard equation (1.1)–(1.3) under the (no-flux) Neumann boundary conditions (1.5), since this gives conservation of mass which is natural in many contexts; see [10] and [15, 19] for details. Note that $\alpha = 0$ again gives the Cahn–Hilliard equation (2.6), now with the boundary conditions (2.8), whilst $\alpha = 1$ gives the nonlocal Allen–Cahn equation (2.10). Numerical computations elucidating the structure of the attractor for this problem with $\alpha = 0$ appear in [4]. Our objective here is simply to show

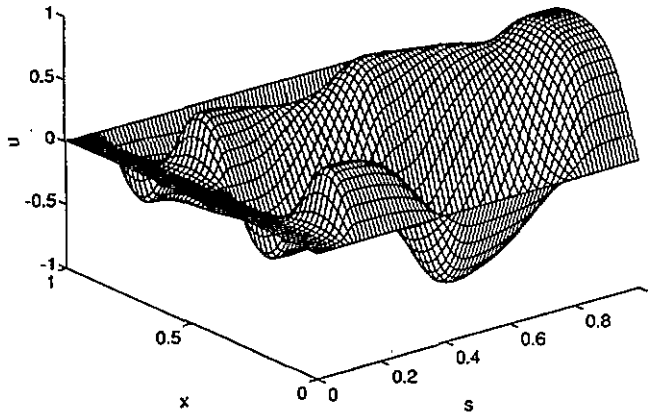

Figure 4.5.(ii). $1/\gamma = 190, \mu_1 = 0.3688, \mu_2 = 0.1850, \alpha = 0$, the Cahn–Hilliard problem. $s = \chi(t)$.

that, as for the Dirichlet case considered in sections 3 and 4, the attractor is insensitive to the parameter α; we do this by computing heteroclinic orbits as a function of α and showing that no qualitative changes occur.

Note that the equilibria are independent of the parameter α. It is easy to see that, from (1.1), (1.5)

$$M = \int_\Omega u(x,t)\mathrm{d}x$$

is independent of t. It is necessary to specify the total mass M to obtain a well-posed equilibrium problem. For any given α the steady states and connecting orbits vary considerably with the choice of the total mass M; see [13, 4] for details. In this paper we will concentrate on the particular case $M = 0.5$ and use the choices $f(u) = u - u^3$ and $\Omega = (0, 1) \subset I\!R$ as in the last section.

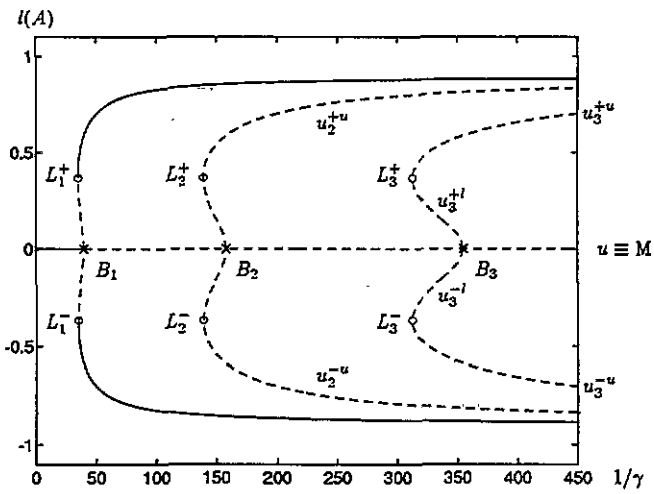

Figure 5.1. Steady state solutions for $M = 0.5$. $I(A) = a_k$, where $|a_k| = \max\{|a_j| : 1 \leqslant j \leqslant N\}$

5.1. Steady state for M=0.5

Figure 5.1 shows the steady-state solutions computed for $M = 0.5$.Note that the local bifurcation points are labelled B_k;the turning points are labelled $L_k^{\pm}$. The equilibria are denoted by $u_k^{+u}, u_k^{-u}, u_k^{+l}, u_k^{-l}$. Here k is determined by B_k, the local bifurcation point of the branch in question. The index, 'u' or 'l' distinguishes solutions above ('upper') or below ('lower') the solution at the turning point $L_k^{\pm}$. The index $\pm$ distinguishes solutions which bifurcate from $u \equiv M$ along the two bifurcating directions at B_k. Solid lines represent stable branches and dashed lines for unstable branches. 'o' are turning points and 'x' are bifurcation points.

5.2. $alpha(u(0)) = u_3^{+l}$, $omega(u(0)) = u_2^{-u}(\gamma)$, $\gamma^{-1} = 340$, $\mu = 1.2646 \times 10^{-2}$

In this case the heteroclinic orbit is a manifold of dimension 2, the first is time and the second we parametrize by introducing

$$\mu = \int_0^1 a_3^2(s)\mathrm{d}s.$$

We can obtain such a connecting orbit for the Cahn–Hilliard equation ($\alpha = 0$) at $\mu = 1.2646 \times 10^{-2}$ by using the computational method described in [3, 4]. By using α as continuation parameter, we perform continuation starting at the viscous Cahn–Hilliard equation ($\alpha = 0$) and finally obtain a connecting orbit for the nonlocal reaction-diffusion equation ($\alpha = 1$). Figures 5.2 (i) and (ii) show the connecting orbits for $\alpha = 1.0$ and $\alpha = 0.0$ respectively.

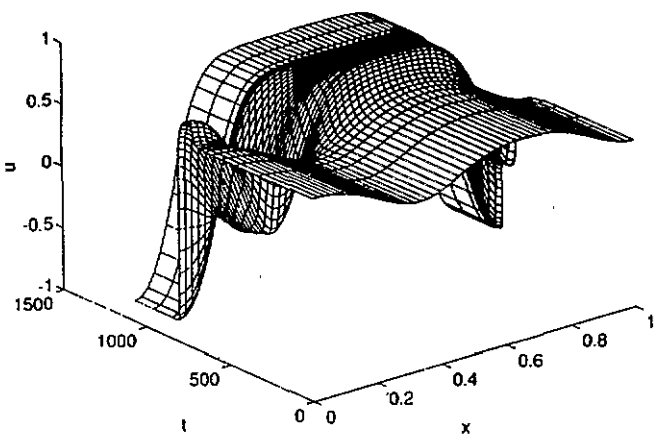

Figure 5.2.(i). $\gamma^{-1} = 340$, $M = 0.5$ and $\mu = 1.2646 \times 10^{-2}$, $\alpha = 1$, the nonlocal reaction-diffusion problem.

The numerical results shown in figures 5.2 indicate the continuity of the attractor for the viscous Cahn–Hilliard equation as α varies; furthermore, the structure of the attractor is again remarkably insensitive to $\alpha \in [0, 1]$. Hence we conjecture that the dynamics of the Cahn–Hilliard equation are closely related to those of the nonlocal reaction-diffusion equation.

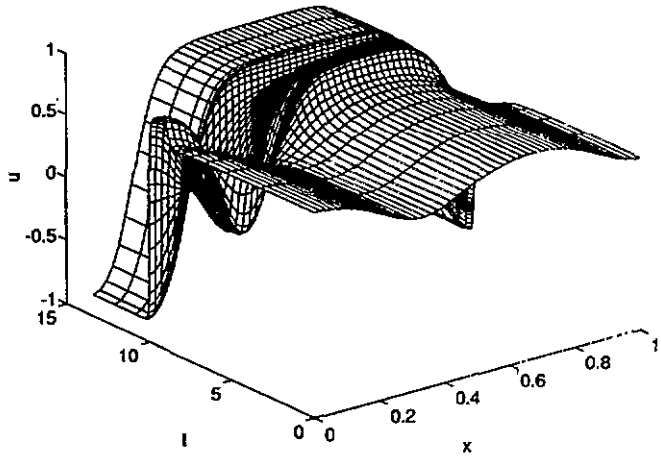

Figure 5.2.(ii). $\gamma^{-1} = 340, M = 0.5$ and $\mu = 1.2646 \times 10^{-2}$, $\alpha = 0$, the Cahn–Hilliard problem.

6. Numerical solution of the initial value problem

Sections 3, 4 and 5 have been devoted to showing that, from a qualitative dynamical systems viewpoint, the values of the parameters α and β play no role in the viscous Cahn–Hilliard equations (1.1)–(1.3). However, in this section we consider the very different mechanisms by which interfaces propagate for $\gamma \ll 1$, depending upon the choices of the parameters α and β. To facilitate comparison with related results concerning the phase-field equations we return to the notation of section 2 and consider the viscous Cahn–Hilliard equation in the form

$$\frac{l}{2}u_t = k\Delta\theta \tag{6.1}$$

$$\alpha u_t = \gamma\Delta u + f(u) + \delta\theta \tag{6.2}$$

subject to Dirichlet or Neumann boundary conditions (2.3) or (2.4). This form is derived from the phase-field model (2.1), (2.2) by setting $c = 0$.

Note that (6.1), (6.2) are related to (1.1), (1.2) through (2.5). It is known, Caginalp and Fife [7], that in the scaling

$$\alpha = \sigma_1\varepsilon^2 \qquad \gamma = \varepsilon^2 \qquad \delta = \sigma_2\varepsilon \qquad 0 < \varepsilon \ll 1 \tag{6.3}$$

the phase-field equations (2.1), (2.2) approximate various sharp interface free boundary problems. For example, in the case of the viscous Cahn–Hilliard equation model (6.1)–(6.2) the leading order term in the asymptotic expansion of $\{u^\varepsilon, \theta^\varepsilon\}$ in powers of ε, which we denote by $\{u, \theta\}$, satisfies the following problem:

$$u(x,t) = \pm 1 \qquad x \in \Omega^{\pm}(t) \tag{6.4}$$

$$k\Delta\theta = 0 \qquad x \in \Omega^{\pm}(t) \tag{6.5}$$

$$lV_n = -[k\nabla\theta]^{\pm}_{-}.\mathbf{n} \qquad x \in \Gamma(t) \tag{6.6}$$

$$\sigma_2\theta = -\sigma_f(\kappa + \sigma_1 V_n) \qquad x \in \Gamma(t) \tag{6.7}$$

$$\Gamma(t) = \partial\Omega^{+}(t) \cap \partial\Omega^{-}(t). \tag{6.8}$$

This is a moving boundary for Laplace's equation. The symbols κ and V_n denote the mean curvature and normal velocity of the interface $\Gamma(t)$ and $\mathbf{n}$ is the unit normal pointing into Ω^+. The sign of κ is chosen to be positive if Ω^- is a ball. The constant σ_f is given by

$$\sigma_f = \frac{1}{2}\int_{-\infty}^{\infty} \{U'(z)\}^2 dz$$

where $U(x)$ is a standing-wave solution of

$$U'' + f(U) = 0 \qquad x \in \mathbb{R} \tag{6.9}$$

subject to boundary conditions which yield a connection between the zeros of $f(\bullet)$. Specifically, with $f(\bullet)$ given by (3.15) we solve (6.9) with $U(x) \to \pm 1$ as $x \to \pm\infty$. Note that, in the scaling (6.3), the analogues of the three cases (i) $\alpha = 0, \beta \neq 0$, (ii) $\alpha \neq 0, \beta = 0$, and (iii) α and β both $\neq 0$, discussed in section 1 are (i) $\sigma_1 = 0, \sigma_2 \neq 0$, (ii) $\sigma_1 \neq 0, \sigma_2 = 0$ and (iii) σ_1 and σ_2 both $\neq 0$.

It is clear by inspection of (6.4)–(6.8) that very different free boundary problems are found in these three cases. In case (i) we obtain a Mullins–Sekerka type problem with the interface governed by the solution of Laplace's equation either side of the interface. This is sometimes referred to as a Hele-Shaw type model. In case (ii) we obtain the pure geometry problem where the interface propagates according to its mean curvature. Case (iii) can be considered as an interpolation between these cases and arises when the temperature at the interfaces between solid and liquid has both curvature dependence and kinetic undercooling ($\sigma_1 \neq 0$). Rigorous results are known for the Allen–Cahn equation in general (e.g. Evans *et al* [20]) and for the phase-field equations either in one dimension, or in two dimensions with radial symmetry (see Stoth [32]). Case (i) has recently been analysed by Alikakos *et al* [1].

In the remainder of this section we briefly describe a computational technique appropriate for the solution of the initial value problem for (6.1),(6.2) and the computation of interface propagation. We then describe numerical results based on this technique. Discretizing (6.1), (6.2) implicitly in time with time step Δt yields the elliptic equations

$$\begin{bmatrix} \Delta t k A & \frac{l}{2} I \\ -\Delta t \delta I & (\alpha I + \gamma \Delta t A) \end{bmatrix} \begin{bmatrix} \theta^m \\ u^m \end{bmatrix} + \begin{bmatrix} 0 \\ -\Delta t f(u^m) \end{bmatrix} = \begin{bmatrix} \frac{l}{2} u^{m-1} \\ \alpha u^{m-1} \end{bmatrix} \tag{6.10}$$

where A represents the operator $-\Delta$ posed on an appropriate space incorporating boundary conditions. In this framework it is possible to consider weak solutions of (6.10). Discretizing in space by a finite difference method or finite element method with piecewise linear elements and mass lumping yields the system

$$\begin{bmatrix} \Delta t k A^h & \frac{l}{2} I \\ -\Delta t \delta I & (\alpha I + \gamma \Delta t A^h) \end{bmatrix} \begin{bmatrix} \underline{\theta}^m \\ \underline{u}^m \end{bmatrix} + \begin{bmatrix} 0 \\ -\Delta t \underline{f}(\underline{u}^m) \end{bmatrix} = \begin{bmatrix} \frac{l}{2} \underline{u}^{m-1} \\ \alpha \underline{u}^{m-1} \end{bmatrix} \tag{6.11}$$

where $-A^h$ is the approximation of the Laplacian with Dirichlet or Neumann boundary conditions as appropriate and $\{\underline{u}^m, \underline{\theta}^m\}$ are vectors of nodal values at time level $m\Delta t$. The superscript h refers to the spatial mesh size. We use the convention that $\underline{f}(\underline{u})$ is the vector with i^{th} component $f(u_i)$ if $\underline{u} = \{\cdots, u_i, \cdots\}^T$. There is an underlying variational structure making (6.11) a computationally viable approximation. First we present a stability result which is only described for the semidiscretization (6.10) but applies also to the fully discrete problem (6.11). The lemma may also be proved for Neumann boundary conditions. Recall C_f given by (3.7) and the Liapunov functional (3.8).

Lemma 6.1. *Let* $\Delta t \leqslant \max(\alpha/C_f, (4\gamma\delta l)/(2kC_f{}^2))$ *and let* $A = -\Delta$ *with* $D(A) = H^2(\Omega) \bigcap H_0^1(\Omega)$. *For each* $u_0 \in H^1(\Omega)$ *there is a unique weak solution* $u^m, \theta^m \in H^1(\Omega) \times H^1(\Omega)$ *of (6.10) for all* $m \geqslant 1$. *This solution satisfies*

$$\mathcal{V}(u^m) + \Delta t \sum_{j=1}^{m} \left\{ \frac{2\delta}{l} |\nabla\theta^j|^2 + \alpha \left| \frac{u^j - u^{j-1}}{\Delta t} \right|^2 \right\} \leqslant \mathcal{V}(u_0). \tag{6.12}$$

Proof. It follows that the first equation of (6.10) becomes

$$\theta^m = -\frac{l}{2k} \mathcal{G}_0 \left(\frac{u^m - u^{m-1}}{\Delta t} \right)$$

where $\mathcal{G}_0$ is introduced at the beginning of section 3 (cf (3.2)), and the second equation of (6.10) becomes

$$\left(\alpha I + \frac{\delta l}{2k} \mathcal{G}_0 \right) \left(\frac{u^m - u^{m-1}}{\Delta t} \right) - \gamma \Delta u^m - f(u^m) = 0. \tag{6.13}$$

Existence follows by a standard variational argument, similar to that in Elliott [15], since (6.13) arises as an Euler–Lagrange equation for the functional

$$\frac{1}{2} \int_\Omega \left\{ \alpha\eta^2 + \frac{\delta l}{2k} \eta \mathcal{G}_0 \eta + \Delta t \gamma |\nabla\eta|^2 \right\} dx + \Delta t \int_\Omega F(\eta) dx - \int_\Omega \eta \left(\alpha I + \frac{\delta l}{2k} \mathcal{G}_0 \right) u^{m-1} dx$$

which is bounded below in $H_0^1(\Omega)$ when f is given by (1.7). To prove uniqueness observe that the difference e between two solutions of (6.10) satisfies (for some $\xi \in H_0^1(\Omega)$)

$$\frac{1}{\Delta t} \left(\alpha I + \frac{\delta e}{2k} \mathcal{G}_0 \right) e - \gamma \Delta e - f'(\xi) e = 0.$$

Taking the inner product of this with e yields

$$\alpha |e|^2 + \Delta t \gamma |\nabla e|^2 + \frac{\delta l}{2k} (e, \mathcal{G}_0 e) \leqslant \Delta t C_f |e|^2 \leqslant \Delta t C_f |\nabla e| (e, \mathcal{G}_0 e)^{1/2}.$$

Thus we obtain uniqueness for Δt sufficiently small. Taking the inner product in $L^2(\Omega)$ of (6.13) with $(u^m - u^{m-1})/\Delta t$ and using an argument identical to that used in Elliott [15] we obtain

$$\mathcal{V}(u^m) + \Delta t \frac{2k\delta}{l} |\nabla\theta^m|^2 + \Delta t \alpha \left| \frac{u^m - u^{m-1}}{\Delta t} \right|^2 \leqslant \mathcal{V}(u^{m-1})$$

yielding the required estimate. □

The nonlinear equations (6.11) can be solved by use of a successive relaxation procedure described in [16]. We now describe numerical computations for the viscous Cahn–Hilliard equation with homogeneous Neumann data. These computations illustrate convergence of solutions to the free boundary problems under the scaling (6.3). We take $f(u) = u - u^3$, so that $\sigma_f = \sqrt{2}/3$. In both one and two dimensional computations, unless stated otherwise, we construct the initial data for the phase variable using the following continuous function

$$U(r,0) = \begin{cases} \hat{u}(r) & 0 \leqslant r < r_1 \\ (U(r_2,0) - \hat{u}(r))(r - r_1)/(r_2 - r_1) + \hat{u}(r) & r_1 \leqslant r < r_2 \\ \tanh((r - R_0)/(\sqrt{2}\varepsilon)) & r_2 \leqslant r \leqslant r_3 \\ (U(r_3,0) - \hat{u}(r))(r - r_4)/(r_3 - r_4) + \hat{u}(r) & r_3 < r \leqslant r_4 \\ \hat{u}(r) & r_4 < r \leqslant L \end{cases} \tag{6.14}$$

where R_0 is the initial position of the interface and

$$r_1 = R_0 - 4\varepsilon \qquad r_2 = R_0 - 3\varepsilon \qquad r_3 = R_0 + 3\varepsilon$$

The value of $\hat{u}(r)$ is given by

$$\hat{u} - \hat{u}^3 + \alpha\theta(r, 0) = 0$$

with $\hat{u}$ taken to be the root closest to -1 if $r < R_0$ and the root closest to $+1$ if $r > R_0$.

Example 1. In one dimension, taking $k = l = 1$, an exact travelling-wave solution of (6.4)–(6.8) is given by

$$\theta(x, t) = \begin{cases} \sigma_f \dfrac{\sigma_1}{\sigma_2} V & x \leqslant s(t) \\ \sigma_f \dfrac{\sigma_1}{\sigma_2} V + V(s(t) - x) & x > s(t) \end{cases}$$

where $s(t) = s_0 + Vt$ denotes the position of the interface $\Gamma(t)$ and $\sigma_f = \sqrt{2}/3$. Notice that this solution breaks down as $\sigma_2 \to 0$, the limit analogous to case (ii) in the remainder of the paper.

Our aim is now to show that, with appropriate initial data and under the scaling (6.3), solutions of the viscous Cahn–Hilliard equation are close to the exact solution of the limiting free boundary problem.

The following data is taken: $\Omega = (0, 0.5)$, $\sigma_1 = 1$, $\sigma_2 = 100/3$, $s_0 = 0.1$, $V = 1$ and $\Delta t = h^2$. At the boundary we impose Neumann conditions. Numerical computations were performed over the time interval $t \in [0, 0.1]$. To illustrate the effect of the initial data U^0 we also take

$$U(x, 0) = \tanh\left(\frac{x - s_0}{\sqrt{2}\varepsilon}\right) \tag{6.15}$$

in addition to taking (6.14) with $R_0 = s_0 = 0.1$. The calculated position of the interface when (6.15) is used is shown in figure 6.1(i) for $\varepsilon = 0.02, 0.01$ and 0.005. Figure 6.1(ii) shows the calculated position of the interface when $\varepsilon = 0.02, 0.01$ and 0.005 and the initial data (6.14) ($r = x$) is used. In both figures the exact position of the interface is shown by the dotted line. Tables 6.1 and 6.2 give results for computations using (6.14) and (6.15) respectively. We measure the error in the temperature at a particular time using the discrete L_2 norm.

Table 6.1. One dimensional experiments with initial data (6.15).

		relative error in interface		error in temperature
ε	h	max	$t = 0.1$	at $t = 0.1$
0.02	1/200	1.33×10^{-2}	9.61×10^{-3}	6.44×10^{-3}
0.01	1/400	6.86×10^{-3}	4.49×10^{-3}	2.83×10^{-3}
0.005	1/800	3.40×10^{-3}	2.16×10^{-3}	1.29×10^{-3}

The results given in tables 6.1 and 6.2 show the numerical solution converging to the exact solution as $\varepsilon \to 0$, with the reduction in the error being $\approx O(\varepsilon)$.

Table 6.2. One dimensional experiments with initial data (6.14)

ϵ	h	relative error in interface max	relative error in interface $t = 0.1$	error in temperature at $t = 0.1$
0.02	1/200	7.29×10^{-3}	7.29×10^{-3}	9.67×10^{-3}
0.01	1/400	3.03×10^{-3}	3.03×10^{-3}	4.22×10^{-3}
0.005	1/800	1.40×10^{-3}	1.40×10^{-3}	1.75×10^{-3}

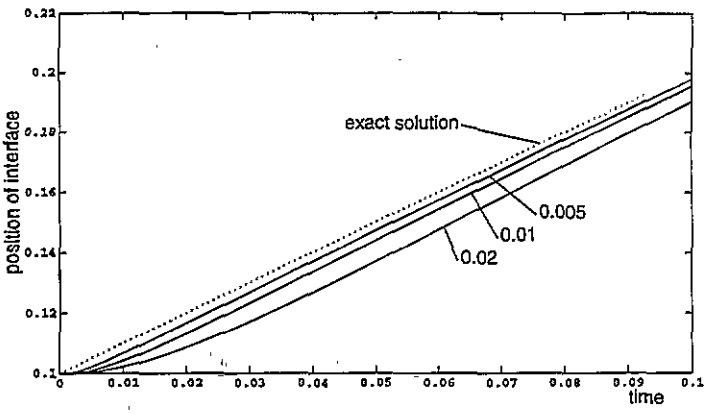

Figure 6.1.(i). Position of interface in one dimensional experiments using initial data(6.15)

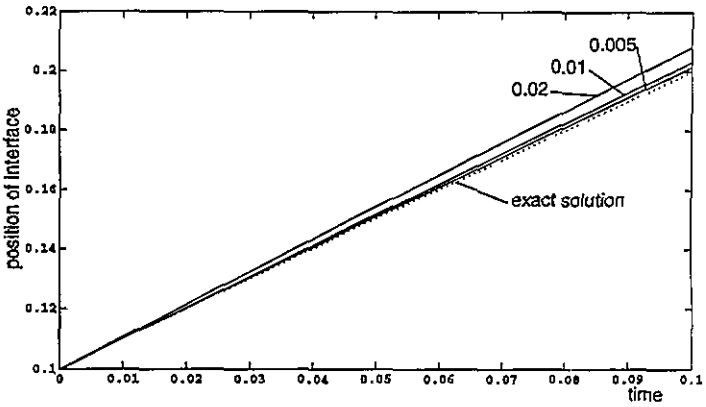

Figure 6.1.(ii). Position of interface in one dimensional experiments using initial data (6.14)

Example 2. We now turn to two dimensional computations. In the radially symmetric case, we denote by $R(t) = R_0 + Vt$ the radial position of the interface $\Gamma(t)$. Then (6.4)–(6.8) become

$$\left.\begin{aligned} &u(r,t) = \pm 1 \\ &(r\theta_r(r,t))_r = 0 \end{aligned}\right\} r \neq R(t)$$

$$\left.\begin{aligned} &\frac{l}{k}\frac{\mathrm{d}R(t)}{\mathrm{d}t} = -\frac{\partial\theta(R(t)^+,t)}{\partial r} + \frac{\partial\theta(R(t)^-,t)}{\partial r} \\ &\sigma_2\theta(R(t),t) = -\sigma_f\left(\frac{1}{R(t)} + \sigma_1\frac{dR(t)}{dt}R(t)\right) \end{aligned}\right\} r = R(t)$$

where $\frac{d}{dt}R(t) = V_n$ and $\kappa = 1/R(t)$. An exact solution in this case is given by

$$\theta(r,t) = \begin{cases} -\frac{1}{3}\left(\frac{1}{\sigma_2}\frac{1}{R(t)} + \frac{\sigma_1}{\sigma_2}V_n\right) & r \leqslant R(t) \\ A(t)\ln r + B(t) & r > R(t) \end{cases}$$

where

$$A(t) = -\frac{l}{2k}\frac{d}{dt}(R(t)^2)B(t) = -A(t)\ln R(t) - \frac{1}{3}\left(\frac{1}{\sigma_2}\frac{1}{R(t)} + \frac{\sigma_1}{\sigma_2}V_n\right).$$

Again we show numerically that the true solution converges to the free-boundary limit under (6.3) as $\varepsilon \to 0$. The following data is taken: $\Omega = (0, 0.5)^2$, $\sigma_1 = 1$, $\sigma_2 = 20\sqrt{2}$, $R_0 = 0.2, V = 1$, $\Delta t = h^2$ and initial data (6.14). We present results when $\varepsilon = 0.01$ and $h = 1/200$ for a uniform mesh. The numerical simulation was run over the time interval $t \in [0, 0.2]$. In figure 6.2 the position of the interface is shown at $t = 0.025(0.025)0.2$. The radial symmetry is clearly seen to be preserved by the numerical computation. In figure 6.3(i) the radial position of the interface is shown while figure 6.3(ii) shows the temperature at the interface. The dotted lines in both figures 6.3 (i) and (ii) correspond to the solution of the free-boundary problem and the solid lines to the computation. Figure 6.3(ii) shows how the temperature at the interface rapidly adjusts to the value corresponding to the free-boundary problem. Note that no initial data is required for the temperature because $c = 0$.

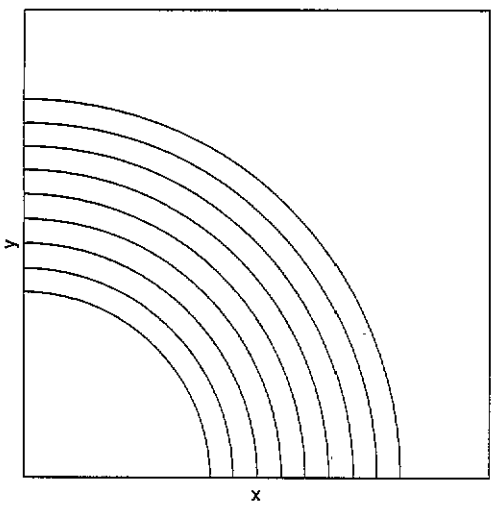

Figure 6.2. Position of interface in radially symmetric case

Finally we perform a series of two-dimensional computations with the scaling (6.3) and using homogeneous Neumann boundary conditions. The initial data in each calculation is a random perturbation of the state $u = 0$ with values distributed uniformly between $+0.05$ and -0.05. In all simulations we took $\Omega = (0, 0.5)^2$. The equation parameters were taken to be $l = k = 1$ along with $\varepsilon = 0.01$ and

(i) $\sigma_1 = 0$ $\sigma_2 = 50$ (Cahn–Hilliard)

(ii) $\sigma_1 = 1$ $\sigma_2 = 0$ (Allen–Cahn)

(iii) $\sigma_1 = 1$ $\sigma_2 = 50$ (Viscous Cahn–Hilliard)

Each simulation was continued until a stationary solution was computed, that is where only one iteration was required to solve the discrete system at each time step and the stationary

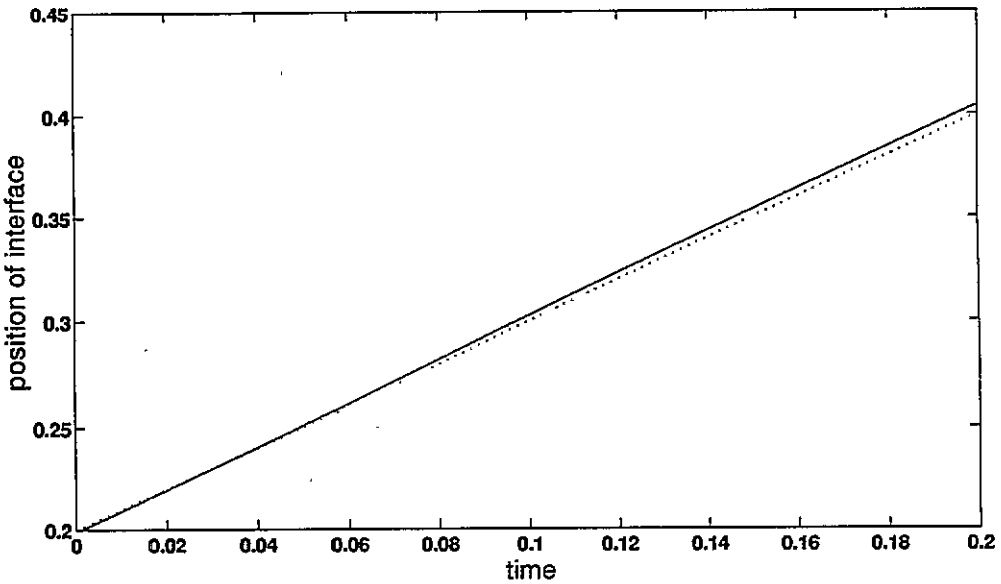

Figure 6.3.(i). Position of interface in radially symmetric case (——) compared to exact value ($\cdots$)

solution persisted, unchanging to machine precision, for a large number of time steps. As an additional check in cases (i) and (iii), we also required that the temperature θ^n was constant in space, up to the prescribed tolerance. From equation (6.1) this ensures that the time-derivative of the phase is negligible. Note that care must be exercised in finding equilibria of these partial differential equations numerically since spatial discretization can introduce spurious equilibria. The ratio of ε to h is crucial in this regard—see [17] and the discussion at the end of the section.

In figure 6.4 the results are illustrated when $h = 0.5/64$ and the same initial perturbation is used. The white areas denote $U > 0$ and the black $U < 0$. In all three simulations a lamella structure rapidly forms, with the domains where $U^n < 0$ and $U^n > 0$ being thin. In time these domains shrink and grow as the interfaces migrate. As can be seen a stationary solution consisting of two strips is reached in the Allen–Cahn and Cahn–Hilliard cases, with the temperature in the Cahn–Hilliard problem being 4.7309×10^{-5}. For the viscous Cahn–Hilliard case a quarter-circle is obtained.

The sharp interface problem (6.4)–(6.8) with Neumann boundary conditions has many equilibria consisting of θ being the constant $-\sigma_f \kappa/\sigma_2$, κ being the mean curvature of the interfaces and the measure of the sets Ω^+ and Ω^- being their initial volumes, which for our choice gives $|\Omega^+| = |\Omega^-| = |\Omega|/2$. It follows that the interfaces for a particular equilibrium are either all straight lines or pieces of circles with fixed radius. Thus it is clear that the equilibrium with minimal interface divides Ω into two strips of equal area with $\theta = 0$ and there are two such equilibria. Furthermore it is known from Γ-convergence theory,

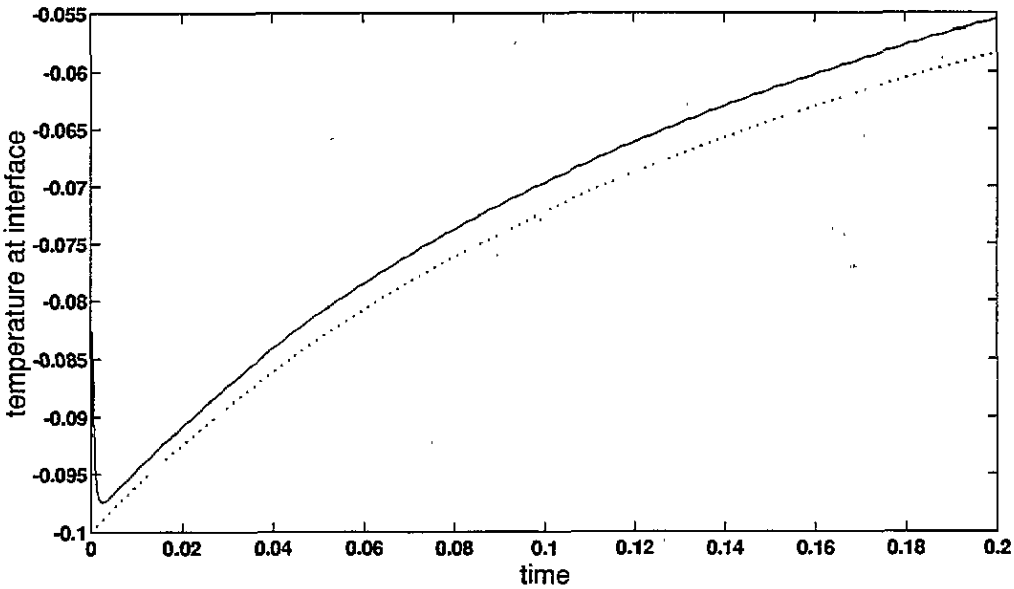

Figure 6.3.(ii). Temperature at interface in radially symmetric case (——) compared to exact value ($\cdots$)

Modica [26], Luckhaus and Modica [25], that the equilibria of (6.1)–(6.2) with minimal energy converges as $\varepsilon \to 0$ to this minimal interface solution. The set of sharp interface equilibria with pieces of circles as interfaces has four minimal interface solutions; each of which consists of a single quarter circle interface located at one of the corners of the square. These exact solutions satisfy

$$\theta = -\frac{\sigma_f}{\sigma_2}\kappa = -\frac{\sigma_f}{\sigma_2}\frac{1}{R_c} \tag{6.16}$$

where R_c is the critical radius of a circle and for our data $R_c = 0.3989$ and $\theta = -0.023\,632$. Our computational steady states in figure 6.4 correspond to these sharp interface steady states. In particular the quarter-circle steady state has the constant equilibrium temperature $\theta = -0.023\,511$ and radius $R_c = 0.3984$ showing close agreement with the exact values.

In order to rule out the possibility that the computed equilibria are spurious, these three simulations were repeated using $h = 0.5/128$, so doubling the number of mesh points appearing in the interfacial region; identical results were obtained in all cases. For the parameters given above the problem was repeated for a number of different initial random perturbations. In all simulations for the Cahn–Hilliard and Cahn–Allen scalings the stationary solution of two strips was obtained, while for the viscous Cahn–Hilliard scaling either a two strips solution or a solution of a quarter circle with critical radius R_c was obtained. Figure 6.5 shows one case where the two strip solution occurs in the viscous Cahn–Hilliard equation, case (ii). A large number of simulations were also performed

using $\varepsilon < 0.01$ with the values of h already described. Such computations are likely to be spurious for sufficiently small ε since the ratio h/ε eventually becomes too large for sufficient resolution of interfaces. Indeed, while the initial stages of the computations resemble those illustrated in figures 6.4 and 6.5, the stationary solutions described above were not always obtained. In general the computed stationary solutions when h/ε is too large had interfaces with small but differing amounts of curvature. Computational experience suggests that, for the nonlinearity $f(u) = u - u^3$, $h \approx \varepsilon/\sqrt{2}$ ensures a sufficient number of mesh points to resolve the interfacial region and exclude spurious solutions. This is consistent with observations made by Caginalp and Socolovsky [8] for the full phase-field model.

We are confident that the computed steady states shown in figure 6.4 are good approximations of steady states of (6.1)–(6.2) and believe that the stability of the two strip steady state is computed correctly. However it is an open question whether the quarter circle steady state is stable.

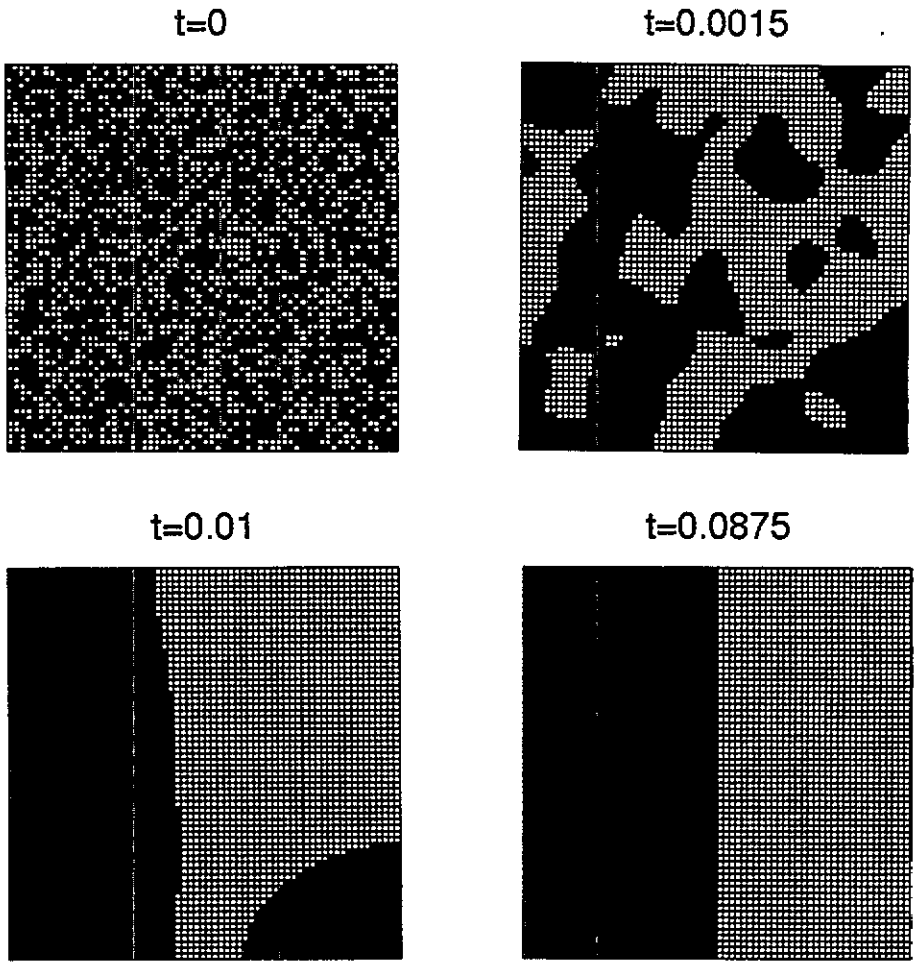

Figure 6.4.(i). Time evolution of Allen–Cahn problem with homogeneous Neumann boundary conditions and $\varepsilon = 0.01$, $\sigma_1 = 1$, $\sigma_2 = 0$.

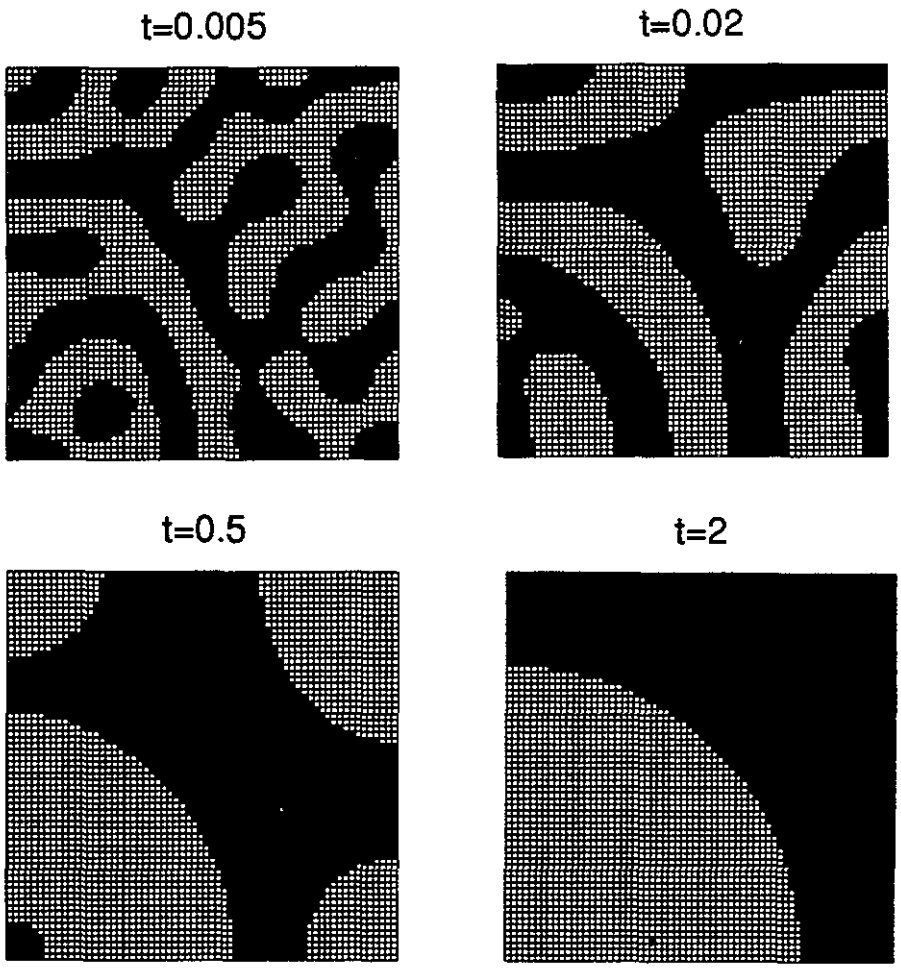

Figure 6.4.(ii). Time evolution of Cahn–Hilliard problem with homogeneous Neumann boundary conditions and $\varepsilon = 0.01$, $\sigma_1 = 0$, $\sigma_2 = 50$.

7. Conclusions

In summary this paper shows by computation and a certain amount of analysis that: (a) from a qualitative dynamical systems viewpoint, the model (1.1)–(1.3) with $\beta = 1 - \alpha$ is independent of $\alpha \in [0, 1]$ for both Neumann and Dirichlet boundary conditions; (b) from the point of view of the detailed physics driving interface propagation in (1.3)–(1.2), the values of α, β and γ are crucial. In a companion paper, [18], we provide theoretical results from a qualitative dynamical systems viewpoint, some of which partially support the computations described here.

Acknowledgment.

The authors thank John Toland, who provided the appendix, for helpful discussions.

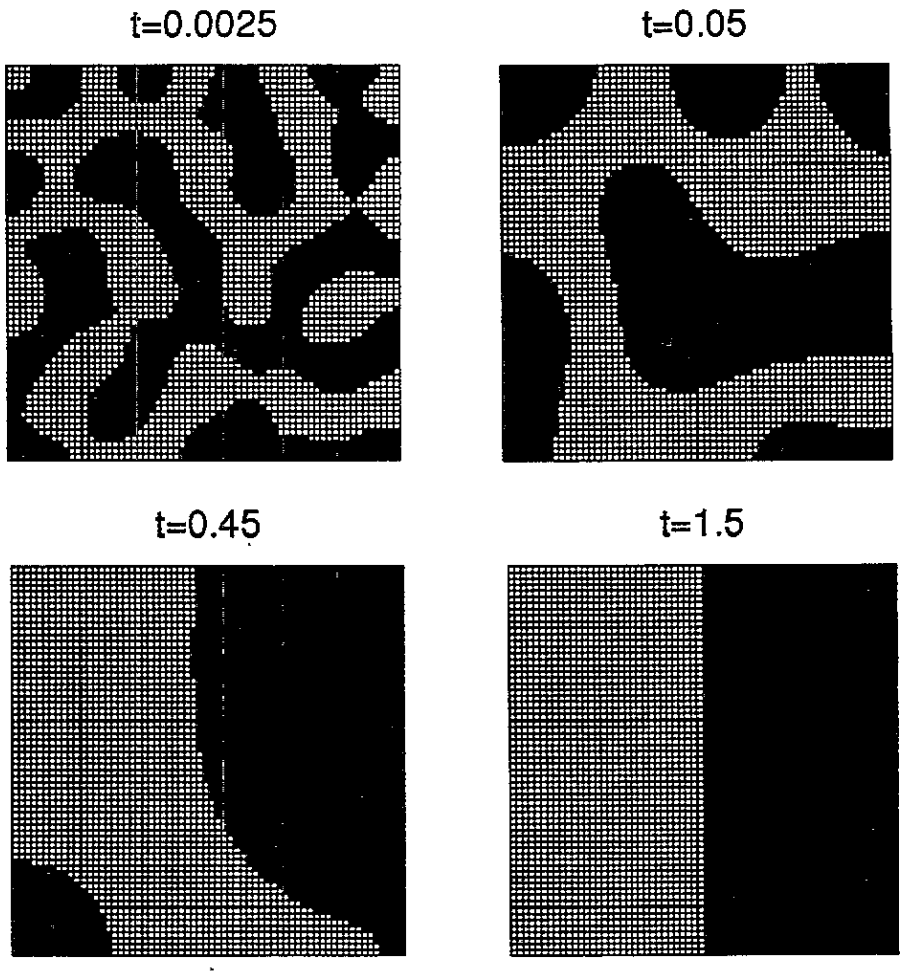

Figure 6.4.(ii). Time evolution of viscous Cahn–Hilliard problem with homogeneous Neumann boundary conditions and $\varepsilon = 0.01$, $\sigma_1 = 1$, $\sigma_2 = 50$.

Appendix

The results given in this appendix are due to J F Toland. They are elementary but we were unable to find them in the literature. The basic result applied in the paper is theorem A, which is proved through the lemmas A1, A2 and A3. Lemma A1 is slightly more general than necessary since it allows L and ML to have zero eigenvalues whilst theorem A refers only to nonzero eigenvalues.

Theorem A. *Suppose L and M are bounded self-adjoint linear operators on a Hilbert space H, L is compact and $(Mx, x) > 0, \forall x \in H \setminus \{0\}$. Then ML, LM, and L have the same number of positive eigenvalues and the same number of negative eigenvalues. The counting of eigenvalues is done using multiplicity. All eigenvalues are real and have equal algebraic and geometric multiplicity (i.e. they are semi-simple).*

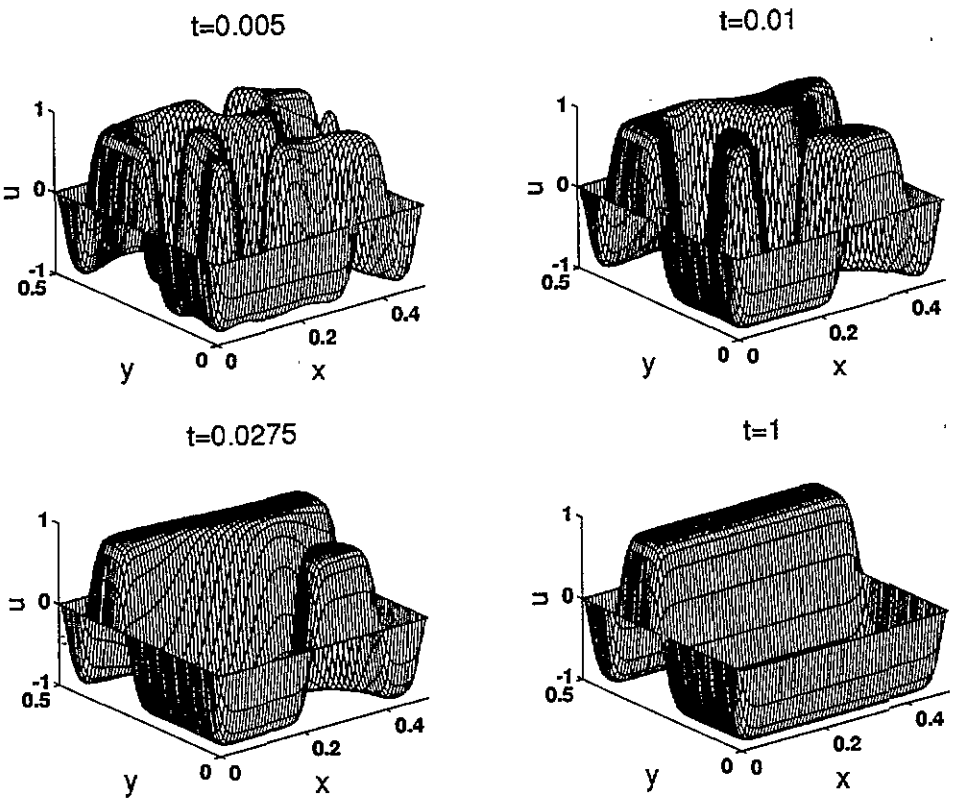

Figure 6.5. Time evolution of viscous Cahn–Hilliard problem with homogeneous Neumann boundary conditions and $\varepsilon = 0.01$, $\sigma_1 = 1$, $\sigma_2 = 50$.

Proof. It suffices to prove the result for ML and L since $(ML)^* = LM$, and for any compact operator P, P and P^* have the same nonzero eigenvalues with the same algebraic and geometric multiplicities. The proof now follows from the following three lemmas. □

Suppose throughout that the remainder of the appendix that H is a Hilbert space and $L, M : H \to H$ are bounded self adjoint operators with $\langle Mx, x\rangle > 0$ for all $x \in H \setminus \{0\}$. Further assumptions are added as needed.

Lemma A.1. *All the eigenvalues of ML are real and semi-simple and*

$$\ker(ML) = \ker(L) \qquad \ker(ML)^2 = \ker(L).$$

bf Proof. Suppose that λ is an eigenvalue of ML. Let $x \neq 0$ be such that $MLx = \lambda x$. Then, if $\lambda \neq 0$, $Lx \neq 0$ and

$$0 < \langle MLx, Lx\rangle = \lambda\langle x, Lx\rangle.$$

Since L and M are self-adjoint, $\langle MLx, Lx\rangle$ and $\langle x, Lx\rangle \in R$. Hence $\lambda \in R$. Thus all the eigenvalues of ML are real. Since M is injective, $\ker(ML) = \ker(L)$.

Now suppose that $MLMLx = 0$, $x \neq 0$. Then $LMLx = 0$ since M is injective. Hence

$$\langle MLx, Lx\rangle = \langle LMLx, x\rangle = 0$$

which implies that $Lx = 0$. Thus $\ker(ML)^2 = \ker(L)$. Since $\ker(ML)^2 = \ker(ML)$ this shows that if 0 is an eigenvalue of ML, it is semi-simple. Now suppose that $\lambda \neq 0$ is an eigenvalue of ML. Say $MLx = \lambda x$ and, seeking a contradiction, that $MLy - \lambda y = x$. Then

$$\begin{aligned} 0 < \langle MLx, Lx\rangle &= \langle MLx,\ LMLy - \lambda Ly\rangle \\ &= \langle MLx, LMLy\rangle - \langle \lambda MLx, Ly\rangle \\ &= \langle \lambda x, LMLy\rangle - \langle \lambda x, LMLy\rangle = 0 \end{aligned}$$

Hence no such a y exists and λ is semi-simple. This completes the proof. □

Lemma A.2. *Suppose that L or M is compact and L has m negative eigenvalues (at least) and n positive eigenvalues (at least). Then ML has at least m negative and n positive eigenvalues. (In all cases eigenvalues are counted using multiplicities. The algebraic and geometric multiplicity are equal.)*

Proof. Let $\{e_1, \cdots, e_m\}$ be an orthonormal family of eigenfunctions corresponding to negative eigenvalues of L. Denote the negative eigenvalue of least absolute value by λ_m so that

$$\lambda_1 \leqslant \lambda_2 \leqslant \ldots, \leqslant \lambda_m < 0.$$

Since M is injective its range, and that of its square root, is dense. Let $\varepsilon > 0$ and let f_j, $1 \leqslant j \leqslant m$ be such that

$$\|M^{\frac{1}{2}} f_j - e_j\| < \varepsilon.$$

Then $\{f_1, \cdots, f_m\}$ is a linearly independent set if $\varepsilon > 0$ is sufficiently small. Let $x = \sum_{i=1}^m \alpha_i f_i$. Then

$$\begin{aligned} \langle M^{\frac{1}{2}} LM^{\frac{1}{2}} x,\ x\rangle &= \langle LM^{\frac{1}{2}} x, M^{\frac{1}{2}} x\rangle \\ &= \langle L \sum_{i=1}^m \alpha_i M^{\frac{1}{2}} f_i \\ &\sum_{i=1}^m \alpha_i M^{\frac{1}{2}} f_i\rangle \\ &= \langle L \sum_{i=1}^m \alpha_i e_i + L \sum_{i=1}^m \alpha_i (M^{\frac{1}{2}} f_i - e_i) \\ &\sum_{i=1}^m \alpha_i e_i + \sum_{i=1}^m \alpha_i (M^{\frac{1}{2}} f_i - e_i)\rangle \\ &\leqslant \sum_{i=1}^m \lambda_i \alpha_i^2 + \varepsilon \|L\|(2+\varepsilon)(\sum_{i=1}^m |\ \alpha_i\ |)^2 \\ &\leqslant (\sum_{i=1}^m \alpha_i^2)\{\lambda_m + \varepsilon(2+\varepsilon)\|L\|m\} \\ &< 0 \end{aligned}$$

if $\varepsilon > 0$ is sufficiently small. Hence the compact, self-adjoint, linear operator $M^{\frac{1}{2}} LM^{\frac{1}{2}}$ is negative on a space of dimension m and so has at least m negative eigenvalues. Say $M^{\frac{1}{2}} LM^{\frac{1}{2}} x = \lambda x$. Then

$$ML(M^{\frac{1}{2}} x) = \lambda (M^{\frac{1}{2}} x).$$

Hence, since $M^{\frac{1}{2}}$ is injective, λ is an eigenvalue of ML. Since $M^{\frac{1}{2}}$ is injective we conclude that ML also has at least m negative eigenvalues.

The argument for positive eigenvalues is obtained by replacing L with $-L$. □

Lemma A.3. *Suppose L is compact and ML has m negative eigenvalues and n positive eigenvalues. Then so does L.*

Proof. Let $\{f_1, \cdots, f_m\}$ be a linearly independent set of eigenvectors of ML corresponding to the negative eigenvalues $\lambda_1 \leqslant \cdots \leqslant \lambda_m < 0$ of L. Then

$$M^{\frac{1}{2}}(M^{\frac{1}{2}} L f_j) = \lambda_j f_j.$$

Hence $f_j = M^{\frac{1}{2}} y_j$ for some $y_j \in H$, and the y_j's form a linearly independent set. Hence

$$M^{\frac{1}{2}}(M^{\frac{1}{2}} L M^{\frac{1}{2}} y_j) = \lambda_j M^{\frac{1}{2}} y_j$$

whence

$$M^{\frac{1}{2}} L M^{\frac{1}{2}} y_j = \lambda_j y_j \qquad 1 \leqslant j \leqslant m.$$

Since $M^{\frac{1}{2}} L M^{\frac{1}{2}}$ is a self adjoint operator, the y_j's corresponding to distinct λ_j are orthogonal. Hence

$$\langle M^{\frac{1}{2}} L M^{\frac{1}{2}} y,\ y\rangle \leqslant \lambda_m \|y\| \qquad \forall y \in Y := \operatorname{span}\{y_1, \cdots, y_m\}.$$

Hence

$$\langle Lz,\ z\rangle < -c\|z\| \qquad \forall z \in Z := M^{\frac{1}{2}} Y = \operatorname{span}\{f_1, \cdots, f_m\}$$

for some $c > 0$. Hence the compact self-adjoint operator L has m negative eigenvalues. The positive eigenvalue problem is done by replacing L with $-L$. □

Note that since lemma A3 may hold for any integer m, the integer m can be interpreted as taking the value infinity.

References

[1] Alikakos N, Bates P and Chen X *Convergence of the Cahn–Hilliard equation to the the Hele–Shaw model.* (Preprint)

[2] Allen S and Cahn J W 1979 A microscopic theory for antiphase boundary motion and its application to antiphase domain coarsing *Acta. Metall.* **27** 1084–95

[3] Bai F, Spence A and Stuart A M 1993 The numerical computation of heteroclinic connections in systems of gradient partial differential equations *SIAM J. Appl. Math* **53** 743–69

[4] Bai F, Spence A and Stuart A M Numerical computations of coarsening in the Cahn–Hilliard model of phase separation *Physica* **78D** 155–65

[5] Beyn W J 1990 The Numerical Computation of Connecting Orbits in Dynamical Systems *IMA J. Numer. Anal.* **9** 379–405

[6] Caginalp G 1986 An analysis of a phase-field model of a free-boundary *Arch. Rat. Anal. Mech.* **92** 205–45

[7] Caginalp G and Fife P 1988 Dynamics of layered interfaces arising from phase boundaries *SIAM J. Appl. Math* **48** 506–18

[8] Caginalp G and Socolovsky E 1991 Computation of sharp phase boundaries by spreading: the planar and spherically symmetric case *J. Comp. Phys.* **95** 85–100

[9] Cahn J W 1968 Spinodal Decomposition *Trans. Metallurg. Soc. of AIME* **242** 166–80

[10] Cahn J W and Hilliard J E 1958 Free energy of a non-uniform system I. Interfacial free energy *J. Chem. Phys.* **28** 258–67

[11] Chafee N and Infante E F 1974 A bifurcation problem for a nonlinear partial differential equation of parabolic type *J. Appl. Anal.* **4** 17–35

[12] Doedel E J and Kernĕvez J P 1986 AUTO: Software for Continuation and Bifurcation Problems in Ordinary Differential Equations *Applied Math. Report* Caltech

[13] Eilbeck J, Furter J and Grinfeld M 1989 On a stationary state characterization of transition from spinodal decomposition to nucleation behaviour in the Cahn–Hilliard model of phase separation *Phys. Lett.* A **135**(1989) 272–75

[14] Eilbeck J, Fife P C, Furter J, Grinfeld M and Mimura M 1989 Stationary states associated with phase separation in a pure material. I. The large latent heat case *Phys. Lett.* A **139** 42–6 **135** 272–75

[15] Elliot C M 1989 The Cahn–Hilliard model for the kinetics of phase separation *'Mathematical Models for Phase Change Problems' ISNM* vol 88 35–74

[16] Elliot C M and Gardiner A R 1993 One dimensional phase-field computations *Numerical Analysis 1993* (proc. July Dundee Conf.) ed D F Griffiths and G A Watson

[17] Elliot C M and Stuart A M 1993 The global dyanmics of discrete semilinear parabolic equations *SIAM J. Num. Anal.* **30** 1622–63

[18] Elliot C M and Stuart A M The viscous Cahn–Hilliard equations, Part II: Analysis, submitted

[19] Elliot C M and Zheng S 1986 On the Cahn–Hilliard equation *Arch. Rat. Mech. Anal.* **96** 339–57

[20] Evans L C, Soner H M and Souganides P E 1992 Phase transitions and generalized motion by mean curvature *Comm. Pure and Appl. Math.* **XLV** 1097–123

[21] Friedman M J and Doedel E J 1991 Numerical computation and continuation of invariant manifolds connecting fixed points *SIAM J. Num. Anal.* **28**) 798–808

[22] Hale J K 1988 Asymptotic Behaviour of Dissipative Systems *Math. Surveys and Mon.* No.25

[23] Henry D 1981 *Geometric theory of Semilinear Parabolic Equations* Lect. Notes in Math. vol 840 (New York: Springer)

[24] Henry D 1985 Some infinite dimensional Morse–Smale systems defined by parabolic differential equations *J. Diff. Equa.* **59** 165–205

[25] Luckhaus S and Modica L 1989 The Gibbs-Thompson relation within the gradient theory of phase transitions *Arch. Rat. Mech. Anal.* **107(1)** 71–83

[26] Modica L 1987 The gradient theory of phase transitions and the minimal interface criterion *Arch. Rat. Mech. Anal.* **98** 123–42

[27] Novick-Cohen A 1988 *On the viscous Cahn–Hilliard equation* Material Instabilitis in Continuum and Related Mathematical Problems ed J M Ball 329–42

[28] Osborne J E 1975 Spectral approximation for compact operators *Math. Comp.* **29** 712–25

[29] Pego R 1989 Front migration in the nonlinear Cahn–Hilliard equation *Proc. Roy. Soc. London Ser.* A **422** 261–78

[30] Penrose O and Fife P 1990 Thermodynamically consistent models of the phase-field type for the kinetics of phase transitions *Physica* **42D** 44–62

[31] Rubinstein J and Sternberg P 1992 Nonlocal reaction-diffusion equations and nucleation *IMA J. Appl. Math.* **48** 249–64

[32] Stoth B E E A model with sharp interface as limit of Phase–Field equations in one space dimension to appear.

[33] Temam R 1988 *Infinite Dimensional Dynamical Systems in Mechanics and Physics* (New York: Springer)

[34] Toland J F 1992 *Private communication*